View metadata, citation and similar papers at core.ac.uk

brought to you by CORE

provided by Lehigh University: Lehigh Preserve

Lehigh University
Lehigh Preserve

Theses and Dissertations

2011

A Numerical Model of Anisotropic Mass Transport Through Grain Boundary Networks

Yibo Wang
Lehigh University

Follow this and additional works at: http://preserve.lehigh.edu/etd

Recommended Citation

Wang, Yibo, "A Numerical Model of Anisotropic Mass Transport Through Grain Boundary Networks" (2011). *Theses and Dissertations*. Paper 1090.

This Thesis is brought to you for free and open access by Lehigh Preserve. It has been accepted for inclusion in Theses and Dissertations by an authorized administrator of Lehigh Preserve. For more information, please contact preserve@lehigh.edu.

A Numerical Model of Anisotropic Mass Transport Through Grain Boundary Networks

by

Yibo Wang

A Thesis

Presented to the Graduate and Research Committee

of Lehigh University

In Candidacy for the Degree of

Master of Science

in

Computational and Engineering Mechanics

Lehigh University

September 2011

Copyright © 2011 Yibo Wang

All Rights Reserved

This thesis is accepted and approved in partial fulfillment of the requirement for the Master of Science.

____

Date

____

Dr. Edmund B. Webb

Thesis Advisor

____

Dr. Gary Harlow

Department Chair

Acknowledgements

First and foremost, to my great parents, Baozhen Wang and Hong Wang, thank you. I am always being inspired, encouraged and supported persistently in this academic road which is full of difficulties, unknown, mystery and surprise.

To Professor Webb, my advisor and mentor, thank you for teaching me all these knowledge from beginning to the end. Your insight and ideas are invaluable to me. You are always my model in the scientific field. Most credits of this thesis belong to your revising and editing. I am grateful eternally.

To my incredible group fellows, Baiou Shi, Haifeng Zheng, Siming Zhang, Murat Al, our friendship lasts forever.

Table of Contents

Acknowledgements iv

Table of Contents v

List of Table viii

List of Figures ix

Abstract 1

1. Introduction 3

1.1 History of Sn plating 3

1.2 Characteristics of Sn whiskers 4

1.3 Factors 8

1.4 Source of compressive stress 13

1.5 Whisker Prevention 16

1.6 Whisker growth theory 17

2. Analytical functions of stress driven mass diffusion 24

2.1 Coble creep and BHT creep 24

2.2 Flux of volume along the grain boundary 29

2.3 Compressive stresses due to adatom insertion into grain boundaries......30
3. Modeling of stress driven mass diffusion......36
3.1 Linear grain boundary model with a constant stress gradient......36
3.2 One Sn grain diffusion model......43
3.3 Equiaxed structure......50
3.3.1 Two dimensional network......50
3.3.2 Unit cell......51
3.3.3 Coordinates......52
3.3.4 Diffusivity......56
3.4 Columnar structure......58
3.4.1 Two dimensional network......58
3.4.2 Unit cell......59
3.4.3 Coordinates......60
3.4.4 Diffusivity......64
4. Equiaxed grain structure testing......66
4.1 Equilibrium diffusivity......66

4.2 Faster diffusivities in central region 70

4.3 10% random segments of faster diffusivities 73

4.4 33% random segments of faster diffusivities 77

4.5 Interpretation and perspective 82

5. Conclusion and Future Work 83

References 85

List of Table

Table 1. Parameters of Coble creep and BHT creep calculations....................................25

Table 2. Parameters of compressive stresses due to adatom insertion into grain boundaries 32

List of Figures

Figure 1.1. Shapes of Sn whiskers 6

Figure 2.1. Effective creep rate vs. applied stress for Coble and BHT creep 26

Figure 2.2. Comparison of Coble creep and BHT creep 27

Figure 3.1. Flowchart of the primary steps in the simulation methodology. 39

Figure 3.2. Initial external stress with constant gradient in linear model. 40

Figure 3.4. Stress versus node number for linear grain boundary model at convergence. 42

Figure 3.5. Initial stress state of single hexagon grain model. 45

Figure 3.6. Stress state of single hexagon system at two different time steps. 48

Figure 3.7. Stress versus node number in single hexagon system. 49

Figure 3.8. Equiaxed structure with a length of 35 μm, and a thickness of 6 μm. 51

Figure 3.9. Unit Cell for equiaxed structure. 52

Figure 3.10. Clarification of the nodes comprising the equiaxed structure in terms of the type of unit cell to which they belong. 53

Figure 3.11. Triple junctions at Node 1 and Node 29 for equiaxed structure.................... 57

Figure 3.12. Model 2D columnar structure with a length of 35 μm, and a thickness of 6 μm. 59

Figure 3.13. Unit cell of columnar structure. 60

Figure 3.14. Clarification of the nodes comprising the columnar structure in terms of unit cell to which they belong. 61

Figure 3.15. Triple junctions, Node 1 and Node 44, in columnar structure. 65

Figure 4.1. Initial stress state and diffusivity of the uniform diffusivity equiaxed network model. 68

Figure 4.2. The total stress state of the uniform diffusivity equiaxed model at two different time steps. 69

Figure 4.3. Initial total stress state and diffusivity of the localized faster diffusivities equiaxed model. 71

Figure 4.4. The stress state of the localized faster diffusivities equiaxed model at two different times. 72

Figure 4.5. Initial total stress state and diffusivity for the equiaxed 10 percent randomly populated fast grain boundaries system. 75

Figure 4.6. The total stress state in the 10 percent randomly populated fast grain boundaries equiaxed model at two different time steps. 76

Figure 4.7. Initial total stress state and diffusivity for the equiaxed, 33 percent randomly populated fast diffusivity grain boundaries....79

Figure 4.8. The total stress state in the 33 percent randomly populated fast grain boundaries equiaxed model at two different time steps....80

Figure 4.9. Total stress state of triple junction nodes at the bottom of the free surface grains, when the first of such nodes reaches 70% of yield....81

Abstract

Tin (Sn) thin films are commonly used in electronic circuit applications as coatings on contacts and solders for joining components. It is widely observed, for some such system, that whiskers – long, thin crystalline structures – emerge and grow from the film. The Sn whisker phenomenon has become a highly active research area since Sn whiskers have caused a large amount of damage and loss in manufacturing, military, medical and power industries. Though lead (Pb) addition to Sn has been used to solve this problem for over five decades, the adverse environmental and health effects of Pb have motivated legislation to severely constrain Pb use in society. People are researching and seeking the reasons which cause whiskers and corresponding methods to solve the problem. The contributing factors to cause a Sn whisker are potentially many and much still remains unknown. Better understanding of fundamental driving forces should point toward strategies to improve a) the accuracy with which we can predict whisker formation, and b) our ability to mitigate the phenomenon.

This thesis summarizes recent important research achievements in understanding Sn whisker formation and growth, both experimentally and theoretically. Focus is then placed on examining the role that anisotropy in grain boundary diffusivity plays in determining whisker characteristics (specifically, whether they form and, if so, where on a surface). To study this aspect of the problem and to enable future studies on stress driven grain boundary diffusion, this thesis presents a numerical anisotropic mass transport model. In

addition to presenting details of the model and implementation, model predictions for a set of increasingly complex grain boundary networks are discussed. Preliminary results from the model provide evidence that anisotropic grain boundary diffusion may be a primary driving mechanism in whisker formation.

1. Introduction

1.1 History of Sn plating

The application of Sn on ironware to protect it against rust is an ancient one. It originated as tinplate in Bohemia in the Middle Ages, from the late thirteenth century to the fourteenth century. The technique of making tinplate spread to nearby regions of Germany, and by the sixteenth century Germany was the only source of tinplate in Europe. Events such as the Thirty Years War interrupted tinplate production, and caused the price of tin wares to increase. Many other European nations, including Great Britain, attempted to start their own tinplate manufacturing industries [1]. In 1728, a successful English tinplate industry was created, and until 1890, tinplate became a British dominated industry, with an output exceeding 13 million boxes of plate, of which 70% were exported to the United States. In 1890, The United States passed the McKinley Tariff bill, which raised the duty level from thirty percent to seventy on tinplate. After this tariff, along with other causes, the US tinplate industry became the largest in the world. It is widely acclaimed that tinware production in the United States was started in Berlin, Connecticut by Scottish immigrant Edward Pattison whose tinware goods were extremely popular due to their ease of use and cleaning. He took on apprentices to help fulfill tinware orders, which later made Berlin, Connecticut, the center of tinware manufacturing in the American Colonies [2].

In contemporary manufacturing science, Sn is a useful metal since it is non-toxic, ductile and not easily oxidized in air. About half of Sn produced is used in solder for joining

pipes or electric circuits where Sn, in the form of an alloy with Pb, accounts for 5 to 70 percent by weight. The remaining Sn production is divided among Sn plating, Sn chemicals, brass and bronze, and other uses [3]. For the food processing industry, Tin-plated steel containers are widely used for food preservation. The first tinplate can for preserving food was manufactured in London in 1813 [4], and now this has become a large part of the market for metallic Sn. The excellent ductility of Sn allows a base metal sheet that has been coated with Sn to be deformed into various shapes without damage to the surface Sn film. The Sn plating process is widely used in the electronics industry to protect both ferrous and nonferrous surfaces from oxidation thus preserving solderability. On Cu electronics, Sn is deposited to reduce oxidation of the Cu conductors and improve its solderability.

1.2 Characteristics of Sn whiskers

As early as the 1950s, Sn whisker growth was recognized as a serious threat to electronic devices since whiskers were observed to randomly grow from surfaces and cause the circuit to short [5]. Similar whiskers are also observed in other materials, including Zinc, Silver, Gold, Cadmium, Aluminum, Pb, Indium, and Sn-Silver-Cu Alloy Systems [6]. In 1966, Bell Laboratories researchers published definitive data showing that adding a few percent Pb into Sn electroplates greatly suppressed the whisker formation [7]. With this straightforward processing modification, the Sn whisker threat was marginalized and Pb-based solder became a mainstay of electronics manufacturing. However, concerns over

adverse environmental and health effects of using lead have caused the whisker problem to re-emerge. In 2003, in Official Journal of the European Union, The European Parliament and the Council of the European Union published a directive to restrict the use of six hazardous substances in manufacturing various types of electrical and electronic equipment, including Pb, Mercury (Hg), Cadmium (Cd), Hexavalent chromium (Cr6+), Polybrominated biphenyls (PBB), and Polybrominated diphenyl ether (PBDE). The directive is commonly referred to as Restriction of Hazardous Substances Directive or RoHS. In this legislation, it was announced that Pb as an alloying element may be present at concentration up to 0.35% in steel, up to 0.4% in aluminum, and up to 4% in Cu by weight [8].

In the United States, California has passed SB 20: Electronic Waste Recycling Act of 2003, or EWRA. This legislation prohibits the sales of electronic devices which are prohibited from being sold under the European Union RoHS directive after January 1, 2007. But it only covers four heavy metals restricted by RoHS and a narrower scale of LCDs, CRTs, and the like. On January 1, 2010, the California Lighting Efficiency and Toxics Reduction Act applies RoHS to general purpose lights, i.e. "lamps, bulbs, tubes, or other electric devices that provide functional illumination for indoor residential, indoor commercial, and outdoor use."[9] Other US states and cities are debating whether to adopt similar laws, and there are several states that have mercury and PBDE bans already. Because of emerging laws of Pb restriction, the use of Pb free solder has increased and, with this, so has the threat of Sn whiskers and potential failure they may cause. Methods for

preventing whisker growth and elucidating fundamental mechanisms of whisker growth are highly active areas of research and development.

The shapes of Sn whiskers have been examined by many researchers. Whiskers may be straight, kinked, hooked or forked (see Figure 1.1). Their outer surfaces are often grooved. Some growths may form as nodules or pyramidal structures instead of high aspect ratio whiskers.

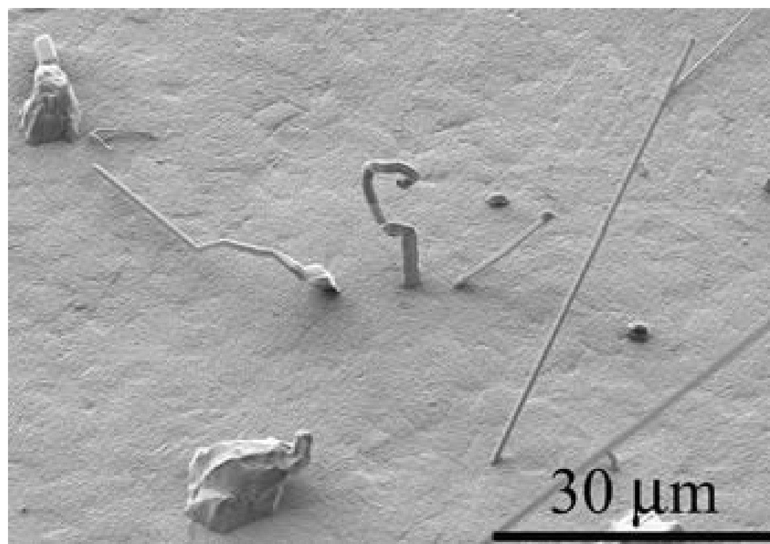

Figure 1.1. Shapes of Sn whiskers. [10]

Mostly Sn whiskers are single crystals with tetragonal crystal structures, however polycrystalline whiskers have been observed [11]. The lengths of Sn whiskers have been observed to grow several millimeters (mm) and in rare instances to lengths in excess of 10 mm. Typical diameters are a few microns with some reports in excess of 10 um and rarely less than 100 nm. Whisker growth rates from 0.03 to 9 mm/year have been reported. Experiments have shown that the incubation period may range from days to years. This characteristic of whisker growth is particularly concerning because experiments to

determine the propensity for a particular process to form whiskers may need to span very long periods of time. The growth is highly variable and is likely to be determined by a complex relationship of factors such as plating methods, plating thickness, substrate materials, grain structure and environmental storage conditions [6].

Damage caused by Sn whisker can be severe. Whiskers can cause short circuits in electrical system; debris or contamination from whiskers that have broken free can interfere with sensitive optics or microelectronic mechanical systems (MEMS), posing a significant threat to reliability. Numerous electronic system failures have been attributed to short circuits caused by Sn whiskers in satellite, military weapons, power plants, medical devices, computers and others.

Several commercial satellites have ceased operation in orbit since the satellite control processors (SCP) were damaged; significant evidence exists indicating failure was caused by short circuits due to Sn whiskers which grew from the pure Sn plated electromagnetic relays. Each satellite has two SCPs, a primary one and a backup one. Failure of both SCPs results in loss of function for the satellite. PanAmSat Corporation's Galaxy VII which launched in 1992, has ceased transmissions due to the loss of the primary SCP in 1998 and the backup SCP in 2000, both failures are accepted to have been caused by Sn whisker induced short circuits. The same as Galaxy VII, Galaxy IV launched in 1993 and lost its backup SCP in 1998; again, failure was concluded to be due to Sn whisker

formation. Also Solidaridad 1 and Galaxy IIIR all lost their primary SCP six years after launch, and very soon the backup SCP stopped working [6].

There are also failures in the military field caused by Sn whiskers. It is reported that in 2000 Raytheon Company's Patriot Missile ran into intermittent misfire problems. The following failure analysis, which included high magnification electron microscopy, pointed out that the cause was Sn whiskers. Other similar incidents have happened involving high profile military products including jet fighter airplanes, the Phoenix air to air missile, the F-15 radar system, and other components in the U.S. military [6].

In medical equipment area, failures because of Sn whisker in artificial pacemakers caused the recall of several models. Failures due to Sn whisker formation have also affected the power industry. In 2005, a sudden nuclear reactor shutdown occurred at Millstone Power Station, CT. With a high powered microscope, a thin filament of metal, barely visible to naked eye, was confirmed to cause the electrical short which gave a false low pressure reading and resulted in an unexpected shutdown [6].

1.3 Factors

It has been concluded that the whisker growth is caused by excess stress induced on the system from a number of intrinsic and extrinsic sources. Extrinsic sources of stress generation include coefficient of thermal expansion mismatch between a Sn film and the

underlying substrate, reactions between the base alloy and the Sn film, and Sn oxidation. Intrinsic sources include microstructural defects (grain boundaries, dislocations), film contaminants such as hydrogen, carbon, oxygen, etc., and porosity [12]. There is a great deal of current research examining these factors and how they affect whisker formation and growth. Several organizations are attempting to devise accelerated test methods to determine a particular plating process's propensity to form Sn whiskers. However, to date, there are no universally accepted test methods for evaluating whisker propensity. Indeed, much of the experimental data compiled to date have produced contradictory findings regarding which factors accelerate or decelerate whisker growth.

Atmosphere pressure is not believed as a contributing factor to affect whisker formation and growth. Whiskers will grow in vacuum as well as earth based atmospheric pressure. Sn whiskers caused failures in satellites while in orbit as well as devices in ambient condition on earth; this provides persuasive evidence that pressure does not have an effect on the whisker formation.

Some observations show that whiskers form more readily in high humidity. Experiments have been done to discover the humidity effect on Sn whisker formation. Dimitrovska et al. [13] used two sets of samples in their experiment. One set of Sn plated brass samples, including a film thickness of 2μm and a film thickness of 5μm, were stored in an environment of high humidity without acidity for 6 month. Another set of Sn plated brass also included a film thickness of 2μm and a film thickness of 5μm, but was stored in

a condition of high humidity with acidity for 6 month. The acidic humidity provides more oxidizing environment than the humidity without acidity. Their results showed that the more oxidizing environment increased the incubation time of the whisker and had a counteracting effect on the whisker growth. The pure humidity is a favorable condition for Sn whisker. The results also showed that the different thicknesses have different whisker growth potentials. In the experiment, thicker films exhibited decreased Sn whisker densities but whiskers were larger in diameter. The authors were unable to determine why a whisker grows at a particular location. The researchers asserted that the particular location of whisker formation is possibly influenced by diffusion of Sn, selective oxidation, and localized condensation of the film. Additionally, while experiments confirm that environmental conditions and Sn film thickness have an effect on the growth of whiskers, they do not directly affect the formation of intermetallic compounds at the interface between a Sn film and the underlying substrate. Since whisker formation is typically observed to occur after intermetallic formation, some aspects controlling the process must be independent of the atmospheric environment.

Storage temperature and thermal cycling are believed to be important factors which have effects on the whisker growth; however, conflicting results exist. Some experiments report that ambient temperatures of approximately 50°C are optimal for whisker formation, while others observe that room temperature (22°C to 25°C) conditions result in faster whisker growth. Whisker growth tends toward zero as temperature exceeds 100°C. As such, this is used as a means of mitigating whisker growth (anneal at 150°C for one hour).

However, some processes cannot exploit this because the relevant device is subject to damage at such elevated temperature. Experiments have been done by L. Sauter et al.[14] to discover if the thermal cycling and storage temperature have effect on whisker formation; they also investigated the effectiveness of widely used whisker resistance methods, (i.e. annealing and Ni interlayer diffusion barriers) to prevent whisker formation. Results showed that the two measures, annealing at 150°C for one hour and Ni interlayer prevented whisker growth during isothermal storage; however, these methods only lessened whisker formation during thermal cycling. The authors concluded the compressive stress generated during isothermal storage is due to inhomogeneous growth of Sn-Cu intermetallic formation at the interface between the Sn film and the underlying Cu substrate. This typically causes mass transport across the interface and into the Sn film, propagating stress. Annealing and diffusion barriers were concluded to effectively mitigate mass transport. The compressive stress generated during thermal cycling was due to different coefficients of thermal expansion of Sn and Cu; as such this source of stress cannot be mitigated by the two methods mentioned above. Because the substrate material is much thicker than the Sn layer, the Sn layer must follow both the thermal expansion and contraction of the base material; thus, at elevated temperatures a compressive stress and at lower temperatures a tensile stress is built up in the Sn layer. Cu and Sn have rather small difference in coefficient of thermal expansion, thus this effect is often neglected. However, by analyzing the microstructure of the sample, the change of the Sn microstructure to globular grains during thermal cycling was observed. This was proposed as the reason why the length of

observed whiskers was shorter and densities were significantly reduced after thermal cycling.

Whiskers grow spontaneously without requiring an applied electric field to encourage their growth. Some recent observations[15] of Sn whisker induced field problems in the commercial sector seem to suggest that an electric field could stimulate whisker growth, but more analysis is required to confirm these effects. NASA’s experiment has demonstrated that whiskers can bend due to the forces of electrostatic attraction thus increasing the likelihood of Sn whisker shorts.

In addition to factors already discussed, other characteristics of Sn whiskers have been observed as follows [16]:

(1) Sn films that are 1-10 μm thick are more susceptible to whisker growth than thinner or thicker films. In particular Sn films <1 or >10 μm thick are relatively immune to whisker growth [17].

(2) The tendency for Sn to whisker is dependent upon the metal or alloy onto which is it deposited; Ni<Fe<Cu<brass [18].

(3) The columnar grain microstructure is more likely to form whiskers than the equiaxed grain microstructure [19].

1.4 Source of compressive stress

The mechanisms by which Sn whiskers grow have been studied for many years. It is generally accepted that Sn whiskers grow as a mechanism of compressive stress relief within a Sn film. The proposed sources of compressive stress include residual stress with Sn plating, intermetallic formation between the Sn deposit and the substrate, Sn surface oxidation and other possible externally applied compressive stress. It is widely believed that stress gradient within the film will drive the flux of Sn to form whiskers at free surface grains to relieve the compressive stress. Other theories contend that whisker growth may be attributed to recrystallization and abnormal grain growth processes affecting the tin grain structure. If such processes dominate Sn whisker generation; it is debatable how they are affected by residual stress in the Sn plated film. Nonetheless, compressive stress is expected to drive the phenomenon.

Residual stresses within a Sn plating can be caused by factors such as the plating chemistry and process. Electroplated finishes appear to be most susceptible to whisker formation purportedly because high purity bright Sn plating processes can introduce greater residual stresses than other plating processes. In Boettinger et al.'s experiment [19], by using the beam deflection method of residual stress analysis, they measured initial residual stresses of three sets of samples, high purity bright Sn, Sn-3%Cu, and Sn-2%Pb. Within 15 minutes of plating, all three electrodeposits had in plane compressive stress. The highest value was 36.5MPa found in 16 μm thick Sn-3%Cu deposits. Sn-Pb deposits have

the lowest compressive stress. In several days, the surfaces of the Sn-Cu deposits develop 50μm contorted hillocks and 200μm whiskers, pure Sn deposits develop 20μm compact conical hillocks, and Sn-Pb deposits remain unchanged. The differences of the initial compressive stresses and the whiskers and hillocks formation among the three sets of experiments were explained by the rapid precipitation of Cu_6Sn_5 or Pb particles within supersaturated Sn grains produced by electrodeposition. The former particles were concluded to stiffen the matrix, producing higher stress and greater whiskering propensity. For Pb particle precipitation, the opposite was concluded to occur.

Intermetallic formation is believed to be the main reason that Sn films experience compressive stress. The diffusion of the substrate material into the Sn plating (or vice versa) can lead to formation of intermetallic compounds, such as Cu_6Sn_5 for Sn deposited on Cu. This alters the lattice spacing in the Sn plating. Intermetallic compound formed from Sn and Cu has a larger molar volume than the mixture of pure Sn and pure Cu, which cause the Sn film to experience compressive stress [16]. The formation of Cu_6Sn_5 intermetallic by reaction between Sn plating and substrate Cu is a relatively slow process controlled by diffusion. Onishi and Fujibuchi [20] have published a measurement of the thickness of the total intermetallic layer including Cu_6Sn_5 and Cu_3Sn between 109°C and 220°C. They obtained $d_{IMC} = \sqrt{Bt}$, where B is a parameter calculated as B= $6.23 \times 10^{-6}\ exp(Q/RT)\ cm^2/s$ and $Q = 57.7\ kJ/mol$, R is gas constant, T is temperature and t represents time. This expression is valid when the thickness of the intermetallic layer is much less than the Sn and Cu layers. Tu and Thompson [21] have measured the growth

rate of intermetallic Cu_6Sn_5 at room temperature and obtained $d_{IMC} = B't$ with $B' = 4 \times 10^{-12}\ cm/s$. This expression is valid for the thickness of intermetallic up to 300nm. Since the rate of intermetallic formation is expected to correlate with propensity for whiskering, more research into intermetallic formation kinetics is warranted.

Sn oxidation and Sn film contamination in the form of hydrocarbons, Cu, hydrogen, etc., tend to increase the whisker propensity. In general, Sn oxide formation could drive whisker growth due to the volume expansion. The molar volume of Sn is 16.2cc/mole, and that of Sn oxide is 21.7cc/mole. Thus, the volume increases about 33 percent after formation of Sn oxide. As oxygen atoms diffuse into the Sn film and form an oxide layer, the relative volume change would form a stress field. However, only a few studies have addressed this issue. The proximity of oxide layers to the free surface complicates descriptions of the resulting stress state. Complicating things further, it has been shown that Sn whiskers can form on oxide free films. Therefore, oxide films may be sufficient to form whiskers, but they are not necessary. If, indeed, they do cause whiskering, how one might relieve Sn whisker growth due to formation of Sn oxide has not been studied yet [22].

Externally applied compressive stresses such as those introduced by torqueing of a nut or a screw or clamping against a Sn coated surface can sometimes produce regions of whisker growth. Bending or stretching of the surface after plating, such as during lead-formation prior to mounting of an electronic component can cause external applied compressive stresses. The external applied compressive stresses can also be introduced by

scratches or nicks in the plating and/or the substrate material introduced by handling, probing, etc. [6].

1.5 Whisker Prevention

Since Sn whisker growth is an irreversible process which couples stress generation and stress relaxation, it is essential to uncouple them in order to prevent whisker growth. In other words, both stress generation and stress relaxation can be explored when developing strategies to prevent whiskers.

Stress generation can be removed by blocking the diffusion of Cu into Sn. The National Electronics Manufacturing Initiative (NEMI) recommends that depositing a Ni interlayer between the Cu substrate and Sn film can suppress whiskers formation. The Ni layers act as a diffusion barrier which prevents the formation of Sn-Cu intermetallic compound. One can also use Sn-Cu intermetallic compound, instead of Ni, as the diffusion barrier. An annealing of the plated Cu substrate above 60°C will lead to the formation of Cu_3Sn, the Cu_3Sn formed between the Cu substrate the Sn finish can serve as diffusion barrier. It is also proposed [23] that by adding Zn in or on the Cu substrate can significantly help to mitigate the formation of long whiskers by suppressing the formation of Cu_6Sn_5. Zn is known to diffuse faster than Cu in Brass. Diffusion of Zn in Sn, however, is slow compared to Cu, due to the atom size of Zn (138 pm) is larger than Cu (128 pm). Also, the effect of Zn has been explained by considering the thermodynamic stability of various

intermetallic compounds relative to Zn. At room temperature, Sn and Zn are completely immiscible. The free energy change associated with the formation of Cu-Zn and Cu-Sn is calculated at room temperature [23]. The value associated with the formation of Cu_6Sn_5 is approximately –5 kJ/mol and that in the formation of Cu_5Zn_8 is approximately –12 kJ/mol. Since the free energy of forming Cu_5Zn_8 is much more negative than that of Cu_6Sn_5, the intermetallic compound will tend to form Cu_5Zn_8.

Although plenty of methods have been proven useful to prevent stress generation, up to now, no solution to remove stress relaxation is given. In other words, how to prevent the creep process or the diffusion of Sn atoms to the whiskers is unknown. This may be accomplished by using another kind of diffusion barrier to stop the diffusion of Sn [24]. For instance, in other materials, some dopant atoms are known to segregate to grain boundaries where they alter diffusivity in the grain boundary. Perhaps such an effect can be exploited in Sn.

1.6 Whisker growth theory

The compressive stress itself provides motivation for whisker growth; however it is necessary but not sufficient for whisker growth. Additional constraints must be placed onto the system to drive whisker formation. Several comprehensive quantitative whisker growth theories have been developed to explain where and how whiskers grow. They are reviewed below.

Boettinger et al. [25] proposed a "creep" model based on whisker growth rate models derived by Tu [26] and Hutchinson et al. [27] referred to as BHT model. Key components of this model are that stress relief occurs via long range grain boundary diffusion and that the form of stress relief will be whiskering if grain boundaries are pinned and hillocks if grain boundaries are mobile. Osenbach [16] discussed four well known creep mechanisms in relation to Sn whiskering: Nabarro-Herring (NH) creep (stress relaxation via lattice diffusion), Coble (C) creep (stress relaxation via grain boundary diffusion), Ashby-Coble (AC) modified creep (stress relaxation via grain boundary diffusion and sliding), and power law (PL) creep (stress relaxation via dislocation glide and / or climb). He [16] concluded that the BHT creep model is capable of reproducing known experimental observations thus providing strong evidence that Sn whisker growth is driven by long range grain boundary diffusion and enhanced by grain boundary pinning. The pinning mechanism could be impurity segregation, surface oxidation, pinning at the free surface, or oxygen grain boundary contamination. Osenbach [16] also discussed the effect on BHT creep mechanism of lattice diffusion, grain boundary diffusion, and lattice and grain boundary diffusion anisotropy. He pointed out that the crystal structure of Sn is anisotropic: the a-axis (<100>) and b-axis (<010>) of the crystal structure are equivalent but $\vec{a}$ and $\vec{b}$ are different from the c-axis. The diffusion coefficient varies along a/b compared to c; the ratio of diffusion coefficient is temperature dependent and activation energy varies in the two directions. Osenbach[16] asserted that this helps explain why whiskers will not grow from microstructures comprised of grains below a critical grain size; this depends on the

crystallographic orientation. NH creep requires that lattice diffusion must occur perpendicular to the grain sidewall, at the grain boundary for grain boundaries to move. In this way, lattice diffusion unpins the microstructure, which prevents whisker growth. Below the critical grain size, lattice diffusion is fast enough on the time scale of whiskering that grain boundaries are mobile and stress relief does not occur via whisker growth. Because lattice diffusion is anisotropic, critical gain size is orientation dependent.

Focusing on the BHT model, Boettinger et al. [19] proposed that Coble creep mechanism (grain boundary diffusion) is the dominant diffusion mechanism to relieve the compressive stress in the deposit. This is believed to be particularly active in Sn because the homologous temperature of Sn at room temperature is 0.6 (i.e. relatively high). A key assumption of the BHT model is that long range diffusion occurs to deliver Sn atoms to whiskering sites. The authors concluded that columnar grain faces have the highest diffusion potentials, oblique grain faces have lower potentials, and grain surfaces parallel to the deposit surfaces have lowest potential. The authors asserted that this is because the diffusion potential is highest for grain faces with surface normal vector perpendicular to the stress gradient, which they assume lies normal to the Sn film free surface. These different diffusion potentials drive the flux of Sn to the oblique grain faces. If there are many oblique grain faces, creep is almost uniform and no whisker will form but there is a uniform increase in thickness of the overall deposit. If there are rarely oblique grain faces, Sn will accumulate on the oblique surface under the free surface in the columnar structures, pushing up the grain to form a whisker. If the grain boundaries are mobile, these oblique

faces will broaden instead so as to form a hillock. If the grain boundaries are immobile, whiskers will form because pinning of the boundaries forces material to extrude from the free surface as a whisker. Boettinger et al. use these arguments to demonstrate that BHT theory also explains the tendency for columnar microstructure to be more whisker prone than equiaxied microstructure.

While BHT theory is considered by many to capture some of the known observations on Sn whiskers, questions remain as to the nature of deformation processes driving stress evolution in Sn thin film. Buchovechy et al. [28] evaluated different mechanisms for the generation of stress in Sn films due to growth of the intermetallic compound. To attempt to explain experimental data on stress evolution during intermetallic growth [30], these different combinations of constitutive behaviors were examined: purely elastic deformation within Sn grains; elastic and plastic deformation within Sn grains; and elastic and plastic deformation within Sn grains combined with diffusion along grain boundaries. The stress driven grain boundary diffusion, coupled with elastic and plastic behavior within Sn grains matched the experimental data. Models that did not include all these mechanisms failed to replicate experiment data. Therefore they concluded this combination provides an effective mechanism for transmitting stress through the thickness of the Sn. The authors also discussed that the effectiveness of grain boundary diffusion as a mechanism for transmitting compressive stress through the film depends on a columnar microstructure in Sn, as well as the presence of a passivating oxide layer. Their models predict that if either of these could be disrupted, strain generated by the growth of

intermetallic compounds could be relaxed via a Coble creep process without producing compressive stress in the Sn, thus reducing the driving force for whisker growth. However, the necessity of oxide layer is debatable. Different opinions exist expressing that the oxide layer is not a necessary condition for Sn whisker formation, so their conclusions appear incomplete.

Many researchers assert that whiskering is a yield mechanism, occurring when stress local to a free surface grain reaches yield for Sn (14.5MPa). However, others assert that whisker growth - or extrusion- may occur for stress below yield. Buchovecky et al. [29] presented finite element simulations which were used to calculate the rate of whisker growth due to intermetallic formation in a Sn film with columnar grain structure on a Cu substrate. The simulation accounted for plastic flow by dislocation motion within the grains, as well as diffusion along grain boundaries. Excess atoms were assumed to enter grain boundaries local to plastic deformation processes. This assumption was based on experimental observation of Chason et al. [30], where electron microscopy was used to clearly reveal dislocation generation local to intermetallic formation regions. The authors provided a mechanism [29] for whisker growth by adding a periodic distribution of soft grains, whose stress at which whiskering occurs (i.e. what the authors called yield stress) is lower than that of the other grains. That is, the authors assumed that whiskers occur at such “soft” grains where crystallography local to the whisker site in such that whiskering occurs for stress below bulk yield. Stress gradients form around the soft grains driving grain boundary diffusion preferentially to soft grains. Strain is then relaxed as the soft grains

accumulate new material and are extruded from the surface of the film. However, the authors did not explain what causes these soft grains to be different from other grains. Indeed, it may be the case that all surface grains can form whiskers at stress below yield. In that case, some other factors must manifest to explain why whiskers form at only certain grains.

This thesis will focus on the question of why whiskers form at only certain grains. What is unique that drives a given grain to be a whiskering site? No assumptions are made about the stress at which whiskering occurs; all grains are considered equivalent; this does not preclude that whiskering in general may occur at stress below yield. Here, though, all of the surface grains are assumed to whisker at the same stress magnitude. What is instead examined here is whether anisotropic grain boundary diffusivities can determine which grains form whiskers. Grain boundary diffusion anisotropy is proposed to exist where diffusion along some grain boundaries is significantly faster than along other grain boundaries. The reason we choose to investigate the role of grain boundary diffusion anisotropy is recent compelling evidence has been presented that significant grain boundary mass transport anisotropy exists in Sn. Using molecular dynamics simulation, Seller et al.[31] demonstrated that some grain boundaries in Sn may exhibit mass transport rates of order 10-20 times diffusivity of other grain boundaries. In addition to this simulation result, other authors have asserted that grain boundary diffusivity anisotropy may play a role [16]. Using this assumption of anisotropic gain boundary diffusivity in Sn, a

simple mass transport model is constructed to explore the influence of grain boundary diffusion anisotropy on Sn whisker formation.

2. Analytical functions of stress driven mass diffusion

Several existing analytical functions have been developed to describe stress driven mass diffusion. Some of them have been used in numerical models of Sn whisker growth. These functions are used to describe Sn film models where Sn atoms diffuse along grain boundaries, driven by stress gradients. In this section, the models of BHT creep and Coble creep are analyzed to discover the critical diffusion distance which distinguishes the two models.

2.1 Coble creep and BHT creep

The mechanism of Coble creep is stress relaxation via grain boundary diffusion, and the mechanism of BHT creep is stress relaxation via long rang grain boundary diffusion and whisker growth. It is useful to explore how the diffusion distance plays a role in distinguishing Coble creep and BHT creep. The two associated quantitative models of strain rate $\dot{\varepsilon}$ are [16]:

(1) Coble creep:

$$\dot{\varepsilon} = \frac{148\Omega\delta D_{gb}\sigma}{\pi RT(GS)^3},$$

(2) BHT Creep:

$$\dot{\varepsilon} = \frac{\Omega \delta D_{gb} \sigma}{RTGSc^2 \ln(\frac{c}{a})},$$

where Ω is the molar volume, D_{gb} is the grain boundary diffusion coefficient, δ is the effective grain boundary width, GS is the grain size, σ is the applied stress, c is the long range diffusion distance, a is the radius of the whisker, R is the gas constant and T is the absolute temperature. Table 1 lists the numerical values for calculating creep rates in Sn; note, creep rate is expected to directly correlate with whisker growth rate.

Table 1. Parameters of Coble creep and BHT creep calculations

Parameter	Value	Definition	Reference
Ω	$1.7 \times 10^{-5}\ m^3/mole$	Molar Volume	[16]
δD_{gb}	$6 \times 10^{-22}\ m^3/s$	Product of effective grain boundary width and diffusion coefficient	[16]
R	$8.314\ J/mole/deg$	gas constant	[16]
GS	10 µm	Grain size	
a	1 µm	Radius of whisker	
T	300 K	Temperature	

For the BHT creep, a Matlab code is created to discover how long range diffusion distance affects the strain rate. Figure 2.1 is shown below to compare a long range diffusion distance of 10 µm and a long range diffusion distance of 200 µm. It can be seen from Figure 2.1 that, for a given long range diffusion distance, the effective strain rate is proportional to the applied stress, which is consistent with the equation. When the long range diffusion distance increases from 10 µm to 200 µm, the effective strain rate

decreases 3 orders of magnitude. Since strain rate is assumed to scale with whisker growth rate, this indicates that whisker growth rate is inversely proportional to diffusion distance. That motivates an exercise to determine the minimum value of the long range diffusion distance. Figure 2.2 shows a comparison between Coble creep model and the BHT creep model, where results for the latter are given for c = 2 μm and c = 10 μm.

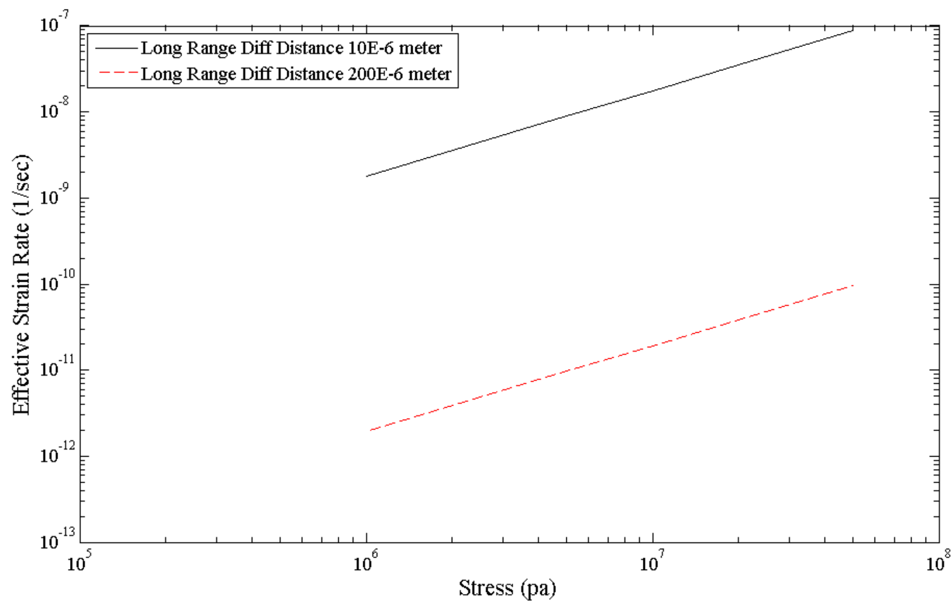

Figure 2.1. Effective creep rate vs. applied stress for Coble and BHT creep

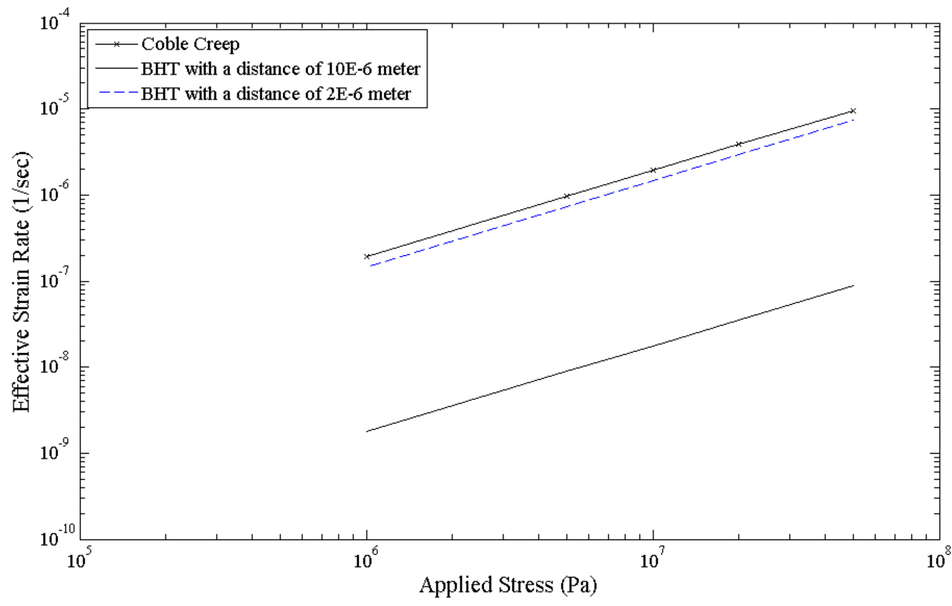

Figure 2.2. Comparison of Coble creep and BHT creep

From Figure 2.2, it can be seen that the plot of Coble creep is very close to the BHT creep with a 2 μm diffusion distance. The exact value of c where two models predict identical behavior can be calculated as following.

Setting them equal,

$$\frac{148\Omega\delta D_{gb}\sigma}{\pi RT(GS)^3} = \frac{\Omega\delta D_{gb}\sigma}{RTGSc^2\ln(\frac{c}{a})},$$

and canceling the same parameters on both sides of the equation,

$$\frac{148}{\pi(GS)^2} = \frac{1}{c^2\ln(\frac{c}{a})}.$$

Rearrangement gives,

$$148c^2 \ln\left(\frac{c}{a}\right) - \pi(GS)^2 = 0\ ,$$

and by using the Matlab fzero function to solve this equation numerically,

$$c = 1.85 \times 10^{-6}\ m.$$

This result indeed satisfies the above expression. Thus, the value of diffusion distance where strain rate predicted for BHT creep is identical to Coble creep is$1.85\ \mu m$.

The interpretation of this analysis in terms of Sn whisker growth is that such a small diffusion distance in the BHT model is of order or less than the film grain size. This implies a very high density of surface grains that grow; in such a situation, whiskering does not occur. Instead, hillocks form or perhaps a uniform film swelling occurs. Only for larger c in the BHT model does one approach typically observed whisker densities. Furthermore, from a given observation of a sample that has grown whiskers, one can compute an amount of material (i.e. volume) that has extruded from the film. Given film dimensions and age of film, one can then compute a corresponding volume strain rate. If the BHT model is applied in such analysis, experimental data are most accurately reproduced using diffusion distance values of order c = 10 μm and larger. Thus, fairly compelling evidence exists that grain boundary diffusion over significant distance drives whisker growth. Alternatively, if a grain boundary system is unpinned, then Coble or AC creep relaxation mechanisms will manifest instead of BHT creep, resulting in less propensity for whisker growth.

2.2 Flux of volume along the grain boundary

For the model presented in this thesis, we assumed that BHT creep mechanism accurately represents phenomena driving whisker growth. Put simply, grain boundary diffusion was assumed to be the primary mass transport mechanism and Sn atoms were assumed to potentially diffuse over significant distance to provide new materials to whisker growth sites. As such, it was necessary to establish a constitutive relationship describing how mass transport occurs along a given grain boundary in a given stress gradient. In their model development, Buchovechy et al. [29] assumed the total flux of volume along the grain boundary $[volume/(l \cdot t)]$ is given by

$$\vec{J_v} = -\frac{\delta D_{gb}}{kT}\nabla\mu \approx \frac{\Omega\delta D_{gb}}{kT}\nabla\sigma_n,$$

where μ is the chemical potential driving the flux of atoms along a grain boundary, which is approximated as $\mu = -\Omega\sigma_n$, Ω is the atomic volume of Sn and σ_n is the normal stress acting across the plane of the grain boundary, δ is the grain boundary width, D_{gb} is the grain boundary diffusivity at temperature T, k is Boltzmann's constant, and the gradient is taken in the plane of the grain boundary. Thus, the volume of atoms that diffuse along a grain boundary can be calculated as

$$V = \frac{\Omega\delta D_{gb}}{kT}\nabla\sigma_n \cdot l \cdot t,$$

where l is the length along the grain boundary, and t is time for diffusion. In the work presented here, the same expression is used to describe mass transport due to a stress gradient. Note this expression can be implemented in either 2D or 3D models fairly simply, albeit with V in a 2D model representing volume per unit thickness in and out of the plane of the model.

2.3 Compressive stresses due to adatom insertion into grain boundaries

Atoms will diffuse from the higher compressive stress region to lower compressive (i.e. more tensile) stress region because of the stress gradient within the film. To model stress driven mass transport through a grain boundary network, one must establish a relationship between excess atoms in a boundary and the resultant compressive stress. Similarly, if atoms are depleted from a grain boundary, tensile stress develops – but to what magnitude? Pao et al. [32] proposed a relationship to determine stress generated by atoms entering grain boundaries from free surface. In their model, the film stress due to adatom incorporation was written approximately as

$$\Delta\sigma_{xx} \approx \frac{-E(a-d)}{L+d} N_X \left(\frac{\pi(a/2)^2}{2L_y h}\right)$$

$$= -\frac{\pi E a^3}{8 L L_y h}\left(1-\frac{d}{a}\right) N_X\,,$$

where E is the film elastic modulus, L is the grain size, L_y was the authors' simulation cell size in y, a is the atomic diameter, h is the thickness of the film, and d is the grain boundary "gap size" in x (i.e., the gap between neighboring grains) The function above can be applied in models of Sn film to calculate the stress change due to atoms diffusion; however, some comments are required. Note that L_y in Pao's model is a dimension of their atomistic scale model system; periodic boundary conditions were applied along this dimension in their model to mimic infinite extent in that direction. Thus the value used by Pao et al. is not directly suitable for modeling stress driven transport in a grain structure scale model. Pao et al. point out that this dimension, in conjunction with their model film thickness, determines the area of their model grain boundary; as such a corresponding length scale in a grain structure model would be of order the spatial discretization size. As will be presented in the following section, we spatially discretize our grain boundary scale model using a discretization value as 0.1μm; other parameters used in the above expression are given in Table 2. Note, grain boundary width δ in expression for Coble creep rate, BHT creep rate, and volume flux is not the same as grain boundary gap size d in Pao's expression; it is instead a measure of the entire grain boundary size perpendicular to the grain boundary plane; δ is typically taken to be some small multiple of a. On the other hand, grain boundary gap size d is related to free volume in a grain boundary and is taken to be smaller than a. Using values in Table 2 we have,

$$\Delta\sigma_{xx} \approx \frac{-E(a-d)}{L+d} N_X \left(\frac{\pi \left(\frac{a}{2}\right)^2}{2L_y h} \right) = -\frac{\pi E a^3}{8 L L_y h} \left(1 - \frac{d}{a}\right) N_X$$

$$= -\frac{\pi \times 50 \times 10^{9}\ \mathrm{Pa} \times (3 \times 10^{-10}\ \mathrm{m})^{3}}{8 \times 1.5 \times 10^{-6}\ \mathrm{m} \times 0.1 \times 10^{-6}\ \mathrm{m} \times 4 \times 10^{-6}\ \mathrm{m}}(1 - 0.9)\mathrm{N_X}$$

$$= -8.84 \times 10^{-2}\ \mathrm{Pa} \cdot \mathrm{N_X}$$

This gives an estimate that each excess atom that diffuses into a grain boundary will cause compressive stress to increase locally by 8.84×10^{-2} Pa. Similarly when one atom diffuses out of an initially equilibrium grain boundary, it will cause a tensile stress evolution of 8.84×10^{-2} Pa.

Table 2. Parameters of compressive stresses due to adatom insertion into grain boundaries

Parameter	Value	Definition	Reference
E	50.0 GPa	Sn film elastic modulus	[28]
a	3×10^{-10} m	Sn atom diameter	
L	1.5 µm	Sn grain size	
L_y	0.1 µm	Length scale in a grain structure model	
h	4 µm	Thickness of the Sn film	
d	0.9a	Gap between neighboring Sn grains	

Chason et al. [33] considered the same system as Pao et al.: atoms entering and exiting grain boundaries from and to a free surface. They provided a more simplified expression

$$\sigma = \frac{E\alpha a^{2}}{Lh}\mathrm{N_{GB}},$$

where L represents the grain size, h is film thickness, E is Sn film elastic modulus, and a is Sn atom diameter, α is a shape factor. Note that authors do not comment on the magnitude of α. However, careful examination of the above expression shows it represents a measure of the strain induced in a grain when an atom enters a grain boundary adjacent to the grain. As such, it is of order the atom size divided by grain size,

$$\alpha = \frac{\text{atom size}}{\text{grain size}} = \frac{10^{-10}\text{m}}{10^{-6}\text{m}} = 10^{-4}.$$

Using the parameters in Table 2,

$$\sigma = \frac{\mathrm{E}\alpha \mathrm{a}^2}{\mathrm{Lh}} \mathrm{N}_{\mathrm{GB}},$$

$$\sigma = \frac{50 \times 10^9\text{Pa} \times 10^{-4} \times (3 \times 10^{-10}\ \text{m})^2}{1.5 \times 10^{-6}\text{m} \times 4 \times 10^{-6}\text{m}} \mathrm{N}_{\mathrm{GB}},$$

$$\sigma = 7.5 \times 10^{-2}\text{Pa} \cdot \mathrm{N}_{\mathrm{GB}}.$$

This answer has the same order of magnitude as the result from Pao's function. Thus, either of these expressions can be used in our following numerical calculations.

2.4 Long range elastic effect

To complete a numerical model of stress driven grain boundary mass transport, sources of stress in our model must be identified. As described above, mass redistribution in a grain boundary network will cause stress evolution. Also, sources external to a film may generate stress in a film grain boundary structure. In addition to these contributions,

long range elastic effects must be evaluated. Consider a system with zero externally applied stress and initially zero stress due to atomic diffusion throughout. The atoms at every point in such a system (i.e. an equilibrium, stress free film) would experience initially zero stress. Now consider atoms being injected into a grain boundary somewhere in the structure; for instance, intermetallic formation near the bottom of a film causes plastic deformation. Because of this, atoms are injected into nearby grain boundaries. This would cause compressive stress generation local to the injection atoms. However, this source of stress also has a long range effect. Elastic deformation fields in a crystal lattice decay relatively slowly with distance from a stress source. In some instances, for instance, stress fields decay as 1/r, where r is distance from the source. To account for this effect in our model, an additional contribution to stress is computed. For clarity, diffusion stress is used to refer to stress generated as a result of mass redistribution inside grain boundaries. Magnitudes given by expressions presented in the preceding section are the stress value at the source of the mass transport effect. The long range elastic effect of the diffusion stress at position j on position i is described by a decay function

$$(\sigma_{L.R.})_i = \frac{(\sigma_{Diffusion})_j}{1 + r_{i,j}/A},$$

where $(\sigma_{L.R.})_i$ is the long range contribution at i from j, $r_{i,j}$ is the distance between position i from j , and A is a length scale parameter. Thus, at each time step, for each position in our model, there is an aggregation of the long range elastic effect from all the other positions due to their diffusion stress,

$$(\sigma_{L.R.})_i = \sum_{j \neq i} \frac{(\sigma_{Diffusion})_j}{1 + r_{i,j}/A}.$$

Because grain boundaries are relatively less ordered regions of a crystal, it is assumed that stress propagates less effectively across grain boundaries than it does through a perfect crystal lattice. Thus, A is chosen to drive initial source stress to 1/10 its original value over a distance equal to grain size in the model. This is a highly simplistic description of long rang elastic effects. However we assert it is sufficient for our model. Note that more complicated descriptions would not influence effects associated with grain boundary diffusion anisotropy because long range stress fields influence all gain boundaries equivalently, as a function of the boundary distance from the stress source. Thus, we conclude the simple description presented is sufficient to explore the role of grain boundary diffusion anisotropy on Sn whisker formation.

3. Modeling of stress driven mass diffusion

In the preceding sections, three mathematical ingredients in our model were presented. Expressions were advanced to describe flux of atoms through a grain boundary network due to stress gradient, stress evolution as a result of mass transport (diffusion stress), and long range elastic effect due to diffusion stress. Having the supporting mathematics, these expressions were combined into a simplified grain boundary diffusion model. Grain boundary networks in our model are discretized into a finite number of positions, or nodes. To present remaining details of our model, two simplified cases are examined below.

3.1 Linear grain boundary model with a constant stress gradient

Consider a model of a grain boundary as a vertical line, which has a length of 4μm, has zero external stress applied at one end and an external stress of 15MPa on the other end. The externally applied stress varies linearly between the ends (Figure 3.2). This stress state is a simplified condition that permits us to explore the model's performance.

To model mass transport along this simplified 1D grain boundary, we first discretize the boundary into segments, where the properties in each segment of the boundary are represented by a node positioned at the segment center. To capture sufficient resolution of the grain boundary network, it was determined that segment length (i.e. nodal

spacing) should be 1/10 the structure's feature size (i.e. the grain size). As such, nodal spacing was taken as 0.1μm throughout this thesis. For each node, the number of excess/depleted atoms in that node's grain boundary segment is recorded, along with that node's corresponding diffusion stress. Mass can exchange only between neighboring nodes and is modeled to do so according to (see Section 2.2)

$$\overrightarrow{J_v} = \frac{\Omega \delta D_{gb}}{kT} \nabla \sigma_{Tot} \ ,$$

where $\nabla \sigma_{Tot}$ now represents the gradient in total stress between two adjacent nodes along the direction of the grain boundary. Thus, the first step in our simulation is the stress gradient computation between all neighboring nodes; Total stress at each node is the sum of,

$$\sigma_{Tot} = \sigma_{Ext} + \sigma_{Diff} + \sigma_{L.R.} \ ,$$

where σ_{Ext} represents externally applied stress, σ_{Diff} is diffusion stress,

$$\sigma_{Diff} = -9 \times 10^{-2} \mathrm{Pa} \cdot \Delta \mathrm{N_{GB}} \qquad \text{(see Section 2.3)},$$

and $\sigma_{L.R.}$ is the sum of long range diffusion stress effects

$$(\sigma_{L.R.})_i = \sum_{j \neq i} \frac{(\sigma_{Diffusion})_j}{1 + r_{i,j}/A} \qquad \text{(see Section 2.4)}.$$

Note that diffusion stress in a node and long range stress in a node due to other nodes' diffusion stress are assumed to act perpendicular to grain boundary walls; however, this is not true for externally applied stress. As such, the geometry of an externally applied field,

relative to a given grain boundary's orientation, must be considered when determining the contribution of σ_{Ext} to σ_{Tot} .

Once the gradient in stress has been computed between all nodal pairs, the second step is to compute the volume flux according to

$$\Delta V = \frac{\Omega \delta D_{gb}}{kT} \nabla \sigma_{Tot} \cdot l \cdot \Delta t \qquad \text{and} \qquad \Delta N_{GB} = \frac{\Delta V}{\Omega},$$

where l is now the simulation discretization length $l = 0.1\mu m$, and Δt is the time in our simulation. Time step is chosen as 1 second, which is small enough not to generate any fluctuations in the numerical calculations. Smaller time step will consume longer time to make the system reach convergence. Longer time steps introduced undesired fluctuations in stress.

With the volume flux between all node pairs computed, the next step is to compute the change in diffusion stress due to mass transport according to

$$\Delta\sigma_{Diff} = \frac{\mathrm{E\alpha a^2}}{\mathrm{Lh}} \Delta N_{GB} = -9 \times 10^{-2}\ \mathrm{Pa} \cdot \Delta N_{GB}.$$

For details on parameters used in above expressions, see Section 2.

After each step in a simulation, our code is constructed to compare the current stress state in the system with the preset criteria. For instance, the code may be constructed to halt after all total stress gradients are below some user set tolerance. From the result of this comparison the code determines whether to continue or not. A flow chart of this process is shown below (Figure 3.1).

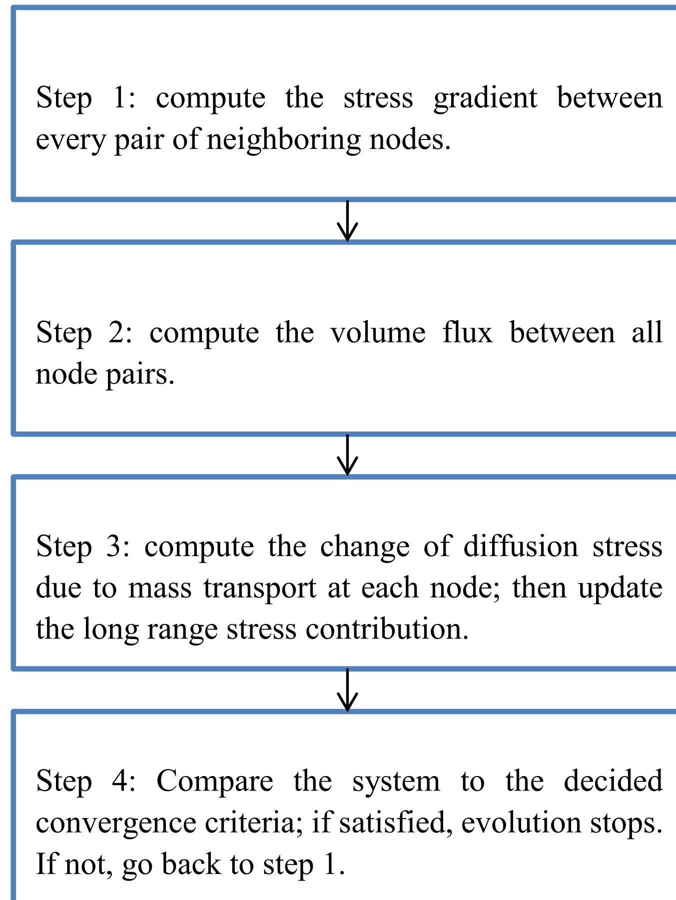

Figure 3.1. Flowchart of the primary steps in the simulation methodology.

In the linear grain boundary model of Figure 3.2, the stress has a constant gradient along the y direction. With a nodal spacing of 0.1μm, the line is divided into 40 segments by 41 nodes. The nodes are labeled from 1 to 41 from bottom to top. The coordinates of the nodes are calculated as

$$x_i = 0\,; \;\; y_i = 0.1\mu m \cdot (i-1)\;, \quad i = 1\ to\ 41$$

With a constant externally applied stress gradient parallel to the linear gain boundary, the stress drop along each segment, which is also the stress difference between each neighboring set of nodes, is uniform. It can be calculated as

$$\frac{d\sigma}{dy} = \frac{-15\ MPa}{4\ \mu m} = -3.75\ MPa/\mu m\ ,$$

thus, the initial external stress of each node can be obtained as seen in Figure 3.2.

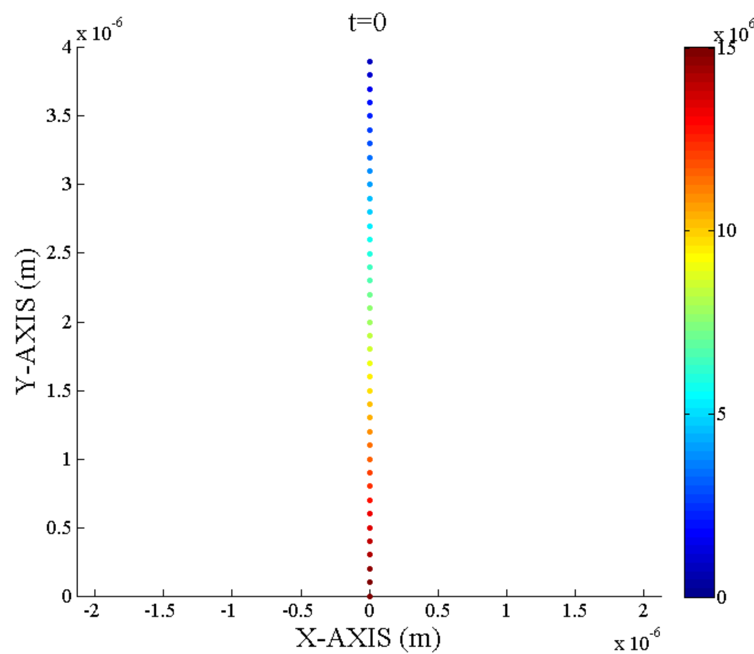

Figure 3.2. Initial external stress with constant gradient in linear model. Note the color bar on the right side shows the stress from 0 to 15MPa.

The initial stress state shows that only external stresses exist along the 41 nodes; this external stress never changes during the diffusion process. The diffusion stress in each node at t=0 is zero; furthermore, long range stress propagation is disregarded in this first test case (i.e. $\sigma_{L.R.} = 0$ at all nodes throughout the simulation). As such, total stress at t=0 is identical to external stress. The number of total atoms in the grain boundary for this model

is assumed to be constant. As such, when atoms leave one node to enter an adjacent node, diffusion stress become more tensile in the former and more compressive in the latter. According to the volume flux expression, atoms will diffuse from the higher compression region to a more tensile stress region, i.e. from the top to bottom in y direction. Because this is a model of a single grain boundary, no anisotropy exists (i.e. δD_{gb} is equal for all nodes). In this case, we iterate the finite difference algorithm until all total stress gradients in the system fall below a pre-set tolerance value; this is the same as halting the simulation when the volume transfer between every pair of neighboring nodes is less than a pre-set tolerance. In terms of volume tolerance, the code is halted when flux between nodes is of order 1 atom per time step, corresponding to stress variations of order 0.1Pa. Figure 3.3 shows that after 156132 times of iteration (156132 s), the system reaches the tolerance value, which we associate with equilibrium; at this point, the total stress of all nodes is equal. From Figure 3.4, the nodes that have larger external stress generate more negative diffusion stress because Sn atoms diffuse from relatively more compressive stress at higher y position to tensile region of stress at lower y position. At equilibrium, diffusion stress versus node number has slope opposite in sign and equal in magnitude to the slope for external stress versus node number. All nodes have total stress equal to 7.5MPa.

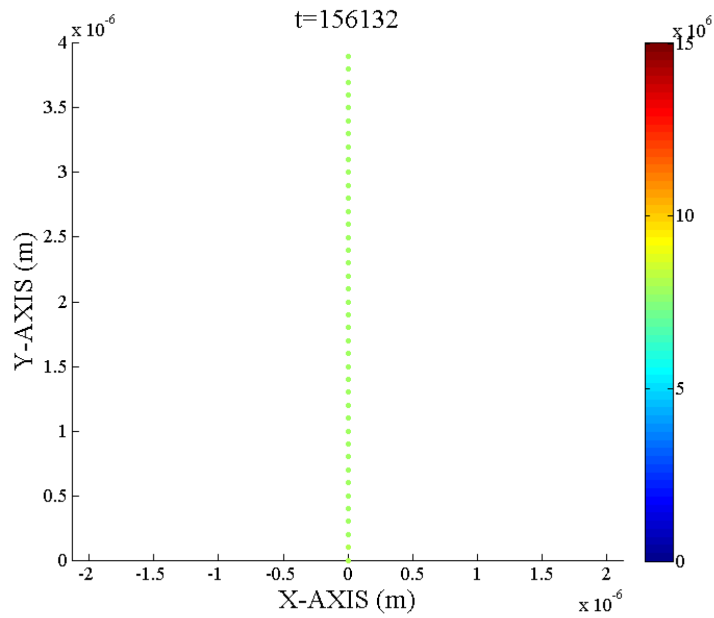

Figure 3.3. Final stress in linear grain boundary model. Note the color bar on the right side shows the stress from 0 to 15MPa.

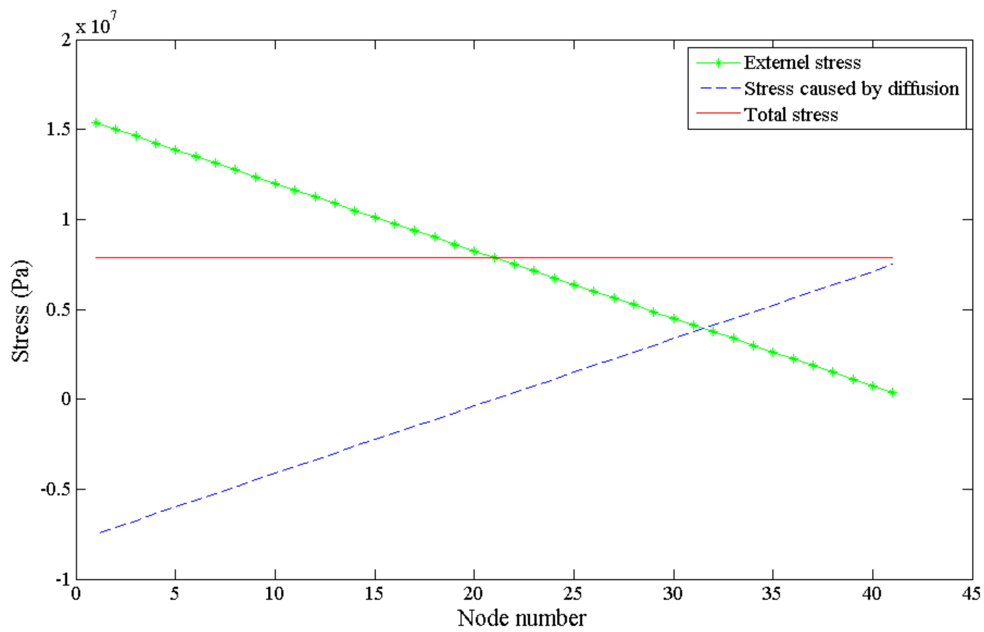

Figure 3.4. Stress versus node number for linear grain boundary model at convergence.

3.2 One Sn grain diffusion model

We next present a single hexagon diffusion network example to mimic one equiaxed Sn grain with a grain size approximately 2 μm. The model is comprised of 80 nodes, shown in Figure 3.5. Again, the bottom node is under an applied external stress of 15MPa and the top node is assumed to have an applied external stress equal to zero. Externally applied stress varies linearly with y-position from bottom to top of the grain boundary model. Again, at t=0, diffusion stress $\sigma_{Diff} = 0$ in all nodes.

The bottom node is labeled (x_1 , y_1) , labels are incremented accordingly along the right hand side to the top node labeled (x_{51} , y_{51}) .The nodes of the left half of the hexagon are labeled from (x_{52} , y_{52}) to (x_{80} , y_{80}) . The x-coordinates of each node are calculated as

$$x_i = 0\,, \quad i = 1\ to\ 11$$

$$x_i = 0.1\mu m \cdot cos30° \cdot (i - 11)\,, \qquad i = 12\ to\ 21$$

$$x_i = 0.1\mu m \cdot cos30° \cdot (21 - 11) = \frac{\sqrt{3}}{2}\mu m\,, \qquad i = 22\ to\ 31$$

$$x_i = \frac{\sqrt{3}}{2}\mu m - 0.1\mu m \cdot cos30° \cdot (i - 31)\,, \qquad i = 32\ to\ 41$$

$$x_i = 0\,, \qquad i = 42\ to\ 51$$

$$x_i = -0.1\mu m \cdot cos30° \cdot (i - 51)\,, \qquad i = 52\ to\ 61$$

$$x_i = -\frac{\sqrt{3}}{2}\mu m\,, \qquad i = 62\ to\ 71$$

$$x_i = -\frac{\sqrt{3}}{2}\,\mu m + 0.1\mu m \cdot cos30° \cdot (i-71)\,, \qquad i = 72\ to\ 80$$

The y-coordinates of the nodes are calculated as

$$y_i = 0.1\mu m \cdot (i-1)\ , \quad i = 1\ to\ 11$$

$$y_i = 1\mu m + 0.1\mu m \cdot sin30° \cdot (i-11)\ , \quad i = 11\ to\ 21$$

$$y_i = 1.5\mu m + 0.1\mu m \cdot (i-21)\ , \quad i = 22\ to\ 31$$

$$y_i = 2.5\mu m + 0.1\mu m \cdot sin30° \cdot (i-31)\ , \quad i = 32\ to\ 41$$

$$y_i = 3\mu m + 0.1\mu m \cdot (i-41)\ , \quad i = 42\ to\ 51$$

$$y_i = 1\mu m + 0.1\mu m \cdot sin30° \cdot (i-11)\ , \quad i = 52\ to\ 61$$

$$y_i = 1.5\mu m + 0.1\mu m \cdot (i-21)\ , \quad i = 62\ to\ 71$$

$$y_i = 2.5\mu m + 0.1\mu m \cdot sin30° \cdot (i-31)\ , \quad i = 72\ to\ 80$$

With the network topology as described, we are able to establish a connectivity map for our calculation. In other words, all node neighbors are easily identified. In this model, we again assume that the stress gradient is constant along y-axis.

$$\frac{d\sigma}{dy} = \frac{-15\ MPa}{4\ \mu m} = -3.75\ MPa/\mu m\,,$$

the initial external stresses of the nodes on the vertical segments can be obtained by

$$\sigma_{ext,i} = 15\ MPa - y_i \cdot 3.75 MPa/\mu m,$$

(i=1 to 11, 22 to 31, 42 to 51, and 62 to 71).

For the nodes on the angled segments, their initial external stresses are calculated by using transformations of stress equation,

$$\sigma_{x'} = \frac{\sigma_x+\sigma_y}{2} + \frac{\sigma_x-\sigma_y}{2}\cos 2\theta + \tau_{xy}\sin 2\theta$$ [34],

in this model, $\sigma_y = 0$, $\tau_{xy} = 0$, $\sigma_{x,i} = 15\ MPa - y_i \cdot 3.75 MPa/\mu m,\ \ \theta = -60°$,

so the external stress for these angled segments nodes should be obtained by,

$$\sigma_{ext,i} = \frac{\sigma_{x,i}}{2} + \frac{\sigma_{x,i}}{2} \cdot \cos(2 \times -60°) = \frac{15\ MPa - y_i \cdot 3.75 MPa/\mu m}{4},$$

i=12 to 21, 32 to 41, 52 to 61, and 72 to 80.

The initial stress state is shown in Figure 3.5.

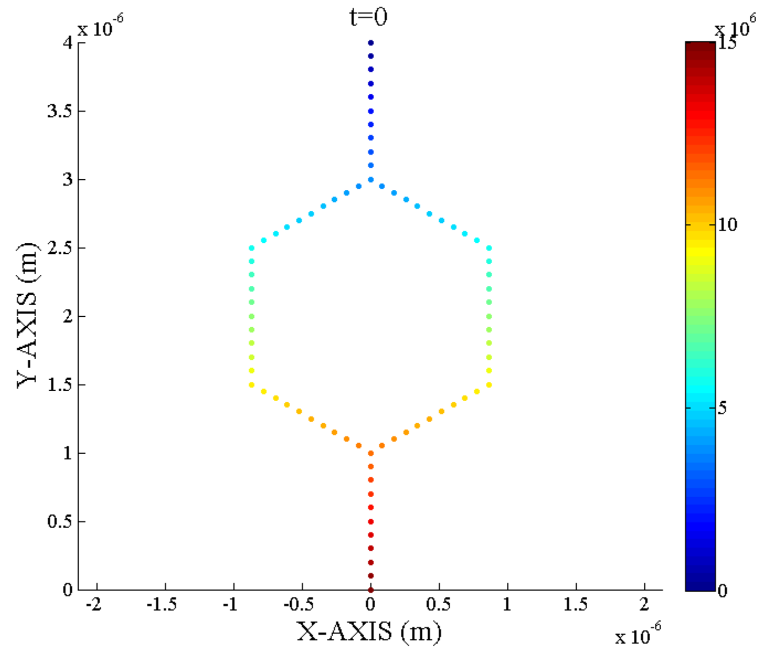

Figure 3.5. Initial stress state of single hexagon grain model. Note the color bar on the right side shows the stress from 0 to 15MPa.

Recall $\sigma_{Diff} = 0$ in all nodes at t=0; as such, $\sigma_{Tot} = \sigma_{Ext}$ in all nodes at t=0. Given the starting stress state, a mass transport simulation was performed. Note, for this test case, long range elastic contributions are disregarded and all grain boundary segments are assumed to have the same diffusivity (represented by δD_{gb}); again no anisotropy exists in this test case. The only sources of stress are from sources external to the film and from atoms diffusing through the grain boundary network. Lastly as before, total number of mobile grain boundary atoms in the system is assumed to be constant.

This model, though seemingly trivial, allows some complexity of grain boundary diffusion to emerge. This model contains junction nodes, which did not exist in the first test case. When two segments join, a node exists at the join position that can be argued to belong to either segment, i.e. a double junction node. Similarly, tripe junction nodes exist. In cases with anisotropy, segments connected by junction nodes can have different δD_{gb}. In such case, δD_{gb} used to compute mass transfer between the junction node and a given segment's node is taken to have the same values as the relevant segment's δD_{gb}. In addition to junction nodes, this mode has grain boundaries with varying inclination. Despite a simple stress gradient and uniform grain boundary diffusivities throughout, initial flux is not uniform. This is due to the relative inclination of vertical segments of the network compared to angled segments. The gradient along the latter is lower in magnitude than along the former, as shown in Figure 3.7. Total stress for each node is shown for two different iteration time steps in Figure 3.6. In Figure 3.7 stress versus node number is shown at t=30,000s and t= 140,359s for nodes 1-51; note, nodes 52-80 (the left

side of the hexagon) give identical results to nodes 12-40 (the right side of the hexagon) As the iteration time step increases from 0 to 140395, the stress at each point reaches convergence (i.e. total stress in all nodes is equal).

Figure 3.7 shows the stress at each node due to externally applied stress σ_{Ext} and stress due to atom diffusion σ_{Diff}. At time zero, excess/depleted atoms due to mass transport are assumed to be zero at all nodes (i.e. equilibrium grain boundary structures). Stress in the grain boundary nodes due to the external gradient ($d\sigma/dx = 0,\ d\sigma/dy = -3.75MPa/\mu m$) is not a simple line but is, instead, linear segments where segments for nodes forming inclined grain boundaries have lower magnitude slope and lower magnitude stress. Double junction nodes are considered vertically aligned. Symmetry gives that triple junction nodes always have vertical inclination. The observed stress distribution in Figure 3.7 is a simple geometric effect. As the system progresses towards equilibrium, the effect of the grain boundary inclination is that significant variations in flux initially manifest. Nonetheless, diffusion quickly equalizes this such that, when the system comes to convergence, the diffusion stress versus node number plot is the mirror shape of the external stress versus node number plot; as such, the total stress at each node is equal.

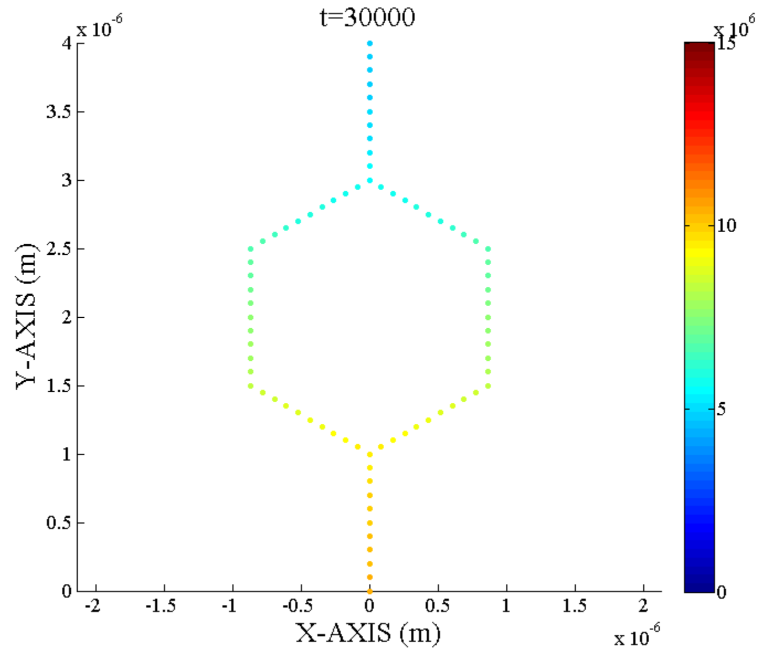

(a) t =30000

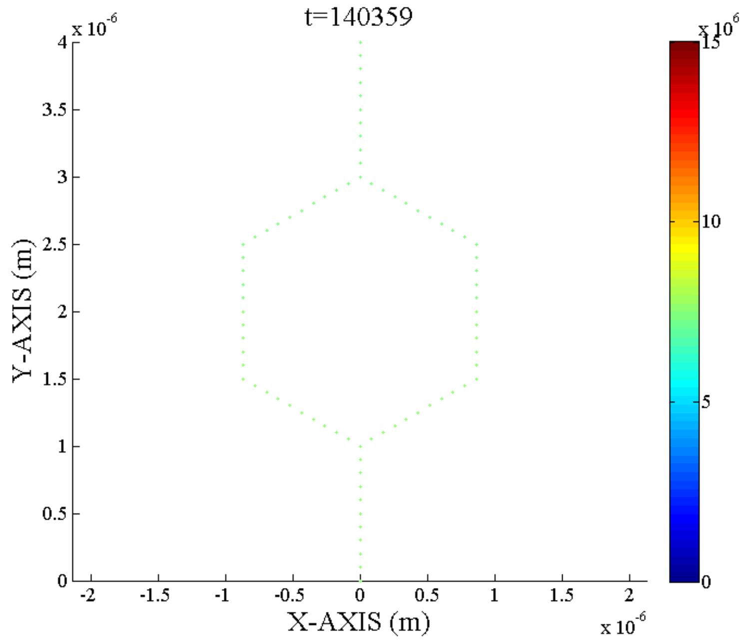

(b) t = 140359

Figure 3.6. Stress state of single hexagon system at two different time steps. Note that color bar on the right side shows the stress from 0 to 15MPa.

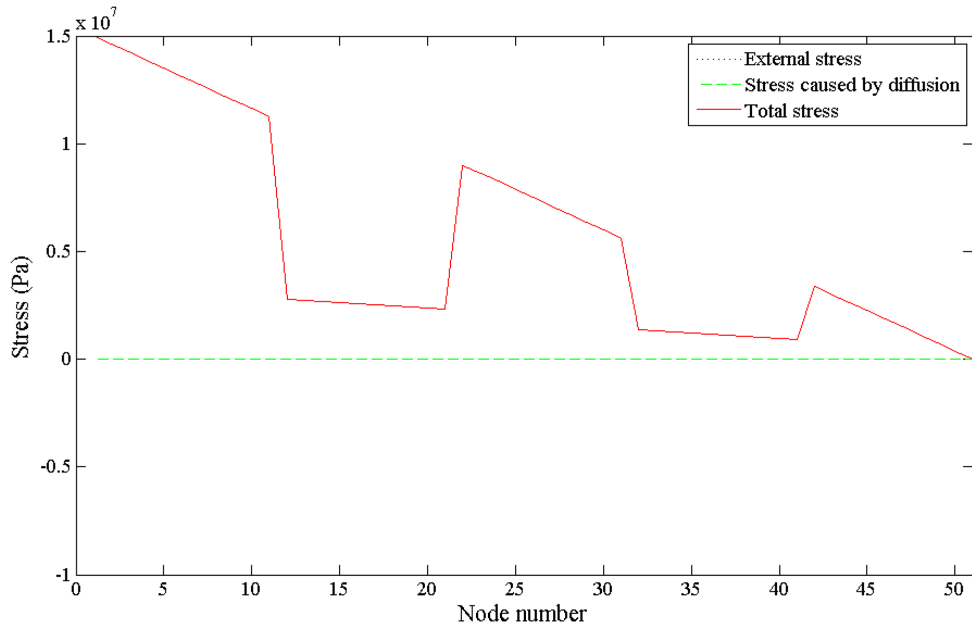

(a) t=0

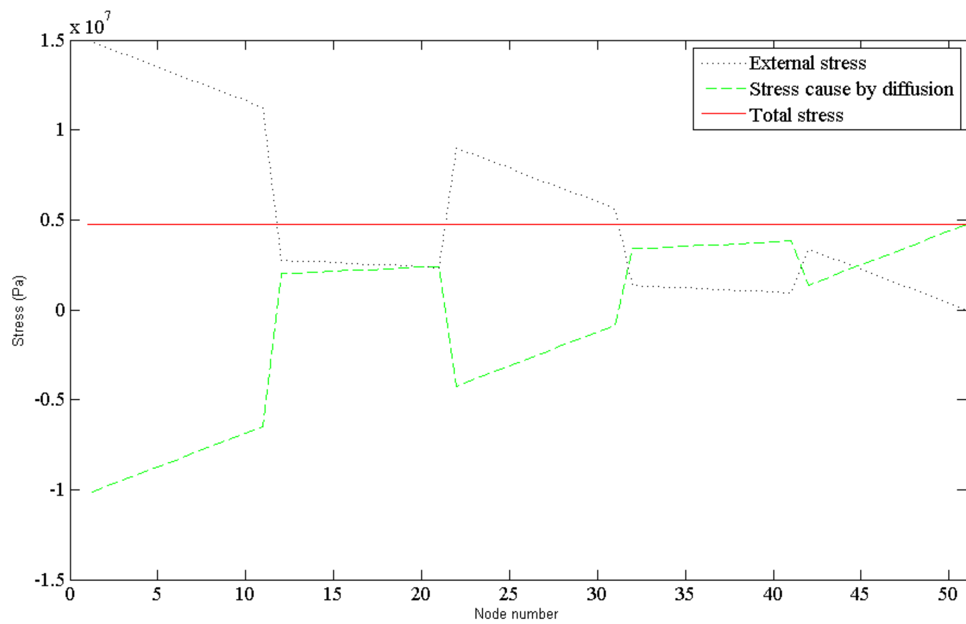

(b) t= 140359

Figure 3.7. Stress versus node number in single hexagon system. Note that the behavior for nodes on the left side of the hexagon was identical to analogous nodes on the right. In (a) the external stress line is identical to the total stress line.

3.3 Equiaxed structure

Having explored a single grain model, we present results from 2 dimensional models of complete grain structure. The model explored is a section of a 2D honeycomb lattice, where the feature (i.e. grain) size is 1μm. Note that all hexagons (i.e. grains) are the same size; as such, this is a 2D model of an ideal equiaxed microstructure. Note this model is 2D, representing a film cross section. All models presented here are 2D. Though our method can be extended into 3D in a fairly straightforward manner, we believe 2D representation permit one to explore the potential for grain boundary diffusion anisotropy to influence propensity for whisker formation and formation location.

3.3.1 Two dimensional network

To be clear, each hexagon shaped grain has edge length equal to 1 μm. The number of Sn grains is decided by Sn film length and thickness. For example, for a model Sn film with a length of 35 μm and a thickness of 6 μm, there are approximately 20 grains along the length direction and 4 grains along the thickness direction, Figure 3.8.

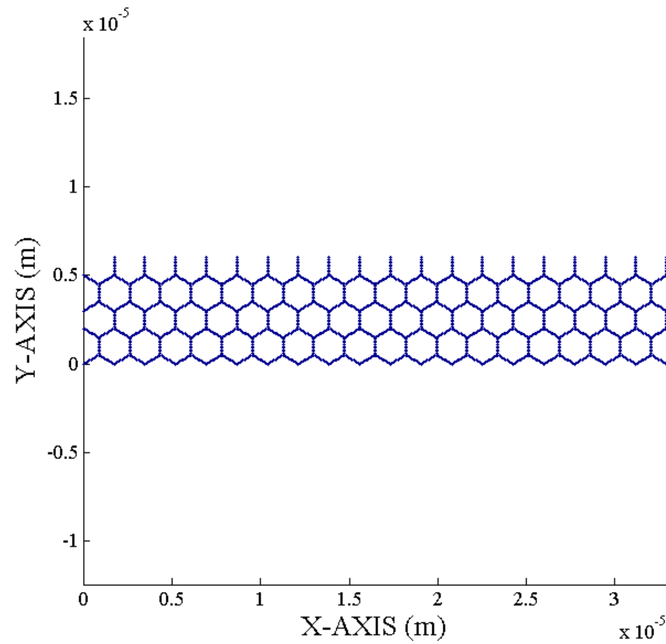

Figure 3.8. Equiaxed structure with a length of 35 μm, and a thickness of 6 μm.

3.3.2 Unit cell

Because we want to model periodic structures, it is useful to define a unit cell for the structure. Each single hexagon inside the equiaxed structure is considered a Sn grain. The unit cell is chosen as half of the hexagon, which is composed of 29 nodes (Figure 3.9). The distance between each two neighboring nodes is again 0.1 μm. Node 1 and Node 29 are two triple junction nodes connected with other unit cells. Accounting for periodicity in the structure, Node 1 has two neighboring nodes in the unit cell to the left (-x) and down (-y) from the unit cell shown in Figure 3.9; in that unit cell the neighboring nodes to Node 1 are Node 19^* and Node 20^* (asterisks are used to denote node numbers in neighboring unit cells

to the one shown in the figure). Similarly, Node 29 has two neighboring nodes in the unit cell to the left (-x) and up (+y) from the unit cell shown in the neighboring unit cell; Node 29's neighbors are Node 10^* and Node 11^*. To complete the connectivity description of a single unit cell, Nodes 20 and 19 are neighbors with Node 1^* in an unit cell to the right (+x) and up (+y) from the unit cell shown. Nodes 10 and 11 are neighbors with Node 1^* in an unit cell to the right (+x) and down (-y) from the unit cell shown.

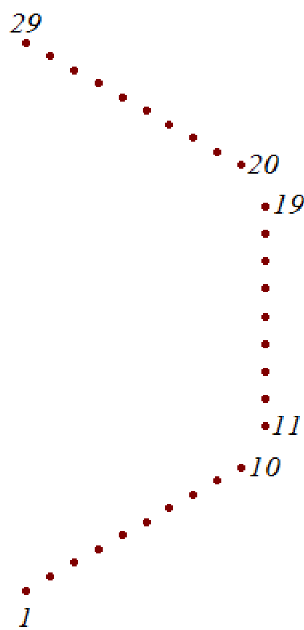

Figure 3.9. Unit Cell for equiaxed structure.

3.3.3 Coordinates

Each node's position in the network is represented by a Matlab three dimension matrix $x(i, ii, iii)$ and $y(i, ii, iii)$, where i represents the position of the unit cell in x-direction, ii represents the position of the unit cell in y-direction, and iii represents the position of the node inside the unit cell. For an equiaxed model shown in Figure 3.10,

the whole network can be distinguished by four different parts. The bottom partial unit cells are located at $ii = 1$ (green part on the bottom of Figure 3.10). The complete unit cells are located from $ii = 2\ to\ 4$ (blue part in Figure 3.10); the partial unit cells at the top are located at $ii = 5$ (green part on top of Figure 3.10); also, several additional nodes required to terminate the structure are located on the top and right boundary (red in Figure 3.10).

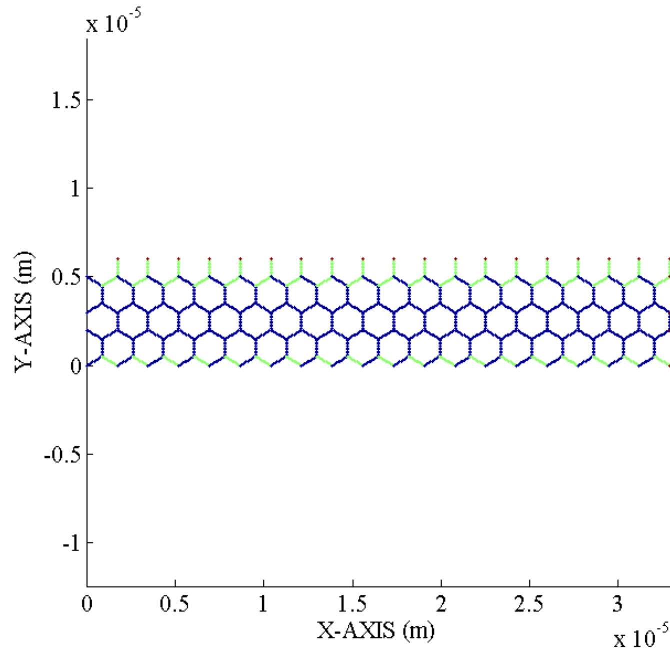

Figure 3.10. Clarification of the nodes comprising the equiaxed structure in terms of the type of unit cell to which they belong.

Thus, the coordinates of all the nodes can be calculated as,

a. Partial unit cells in the bottom $i = 2\ to\ 20, ii = 1, iii = 20\ to\ 29$

$$x(i, 1, iii) = 1\mu m \times sin60° \times (i - 1) \times 2 - 0.1\mu m \times sin60° \times (iii - 19)$$

$$y(i,1,iii) = 0.1\mu m \times cos60° \times (iii - 19)$$

b. complete cells in the middle of the network $i = 2\ to\ 20$, $ii = 2\ to\ 4$,

if ii is even

$$x(i,ii,iii) = 1\mu m \times sin60° \times (i-2) \times 2 + 0.1\mu m \times sin60° \times (iii - 1),$$

$$iii = 1\ to\ 10$$

$$x(i,ii,iii) = 1\mu m \times sin60° \times [(i-2) \times 2 + 1], \qquad iii = 11\ to\ 19$$

$$x(i,ii,iii) = 1\mu m \times sin60° \times [(i-2) \times 2 + 1] - 0.1\mu m \times sin60° \times (iii - 19),$$

$$iii = 20\ to\ 29$$

if ii is odd

$$x(i,ii,iii) = 1\mu m \times sin60° \times [(i-2) \times 2 + 1] + 0.1\mu m \times sin60° \times (iii - 1),$$

$$iii = 1\ to\ 10$$

$$x(i,ii,iii) = 1\mu m \times sin60° \times [(i-2) \times 2 + 2], \qquad iii = 11\ to\ 19$$

$$x(i,ii,iii) = 1\mu m \times sin60° \times [(i-2) \times 2 + 2] - 0.1\mu m \times sin60° \times (iii - 19),$$

$$iii = 20\ to\ 29$$

$$y(i,ii,iii) = (1\mu m + 1\mu m \times sin30°) \times (ii - 2) + 0.1\mu m \times sin30° \times (iii - 1),$$

$$iii = 1\ to\ 10$$

$$y(i,ii,iii) = (1\mu m + 1\mu m \times sin30°) \times (ii-2) + 1\mu m \times sin30° + 0.1\mu m \times (iii-10), \qquad iii = 11\ to\ 19$$

$$y(i,ii,iii) = (1\mu m + 1\mu m \times sin30°) \times (ii-1) + 0.1\mu m \times sin30° \times (iii-19), \qquad iii = 20\ to\ 29$$

c. Partial unit cell on the top $i = 2\ to\ 20, ii = 5, iii = 1\ to\ 19$

$$x(i,ii,iii) = 1\mu m \times sin60° \times (i-2) \times 2 + 0.1\mu m \times sin60° \times (iii-1), \qquad iii = 1\ to\ 10$$

$$x(i,ii,iii) = 1\mu m \times sin60° \times (i-2) \times 2 + 0.1\mu m \times sin60° \times 10, \qquad iii = 11\ to\ 19$$

$$y(i,ii,iii) = (1\mu m + 1\mu m \times sin30°) \times (ii-2) + 0.1\mu m \times sin30° \times (iii-1), \qquad iii = 1\ to\ 10$$

$$y(i,ii,iii) = (1\mu m + 1\mu m \times sin30°) \times (ii-2) + 1\mu m \times sin30° + 0.1\mu m \times (iii-10), \qquad iii = 11\ to\ 19$$

d. Additional nodes which complete the network

d-1. Nodes on the top $i = 3\ to\ 20, \ ii = 6$

$$x(i,6,1) = 1\mu m \times sin60° \times (i-2) \times 2$$

$$y(i,6,1) = (1\mu m + 1\mu m \times sin30°) \times 4$$

d-2. Nodes on the right boundary when ii is even,

$$x(21, ii, 1) = 1\mu m \times sin60° \times (20 - 1) \times 2$$

$$y(21, ii, 1) = (1\mu m + 1\mu m \times sin30°) \times (ii - 2)$$

$$x(21, ii, 29) = 1\mu m \times sin60° \times (20 - 1) \times 2$$

$$y(21, ii, 29) = (1\mu m + 1\mu m \times sin30°) \times (ii - 1) + 1\mu m \times sin30°$$

3.3.4 Diffusivity

The diffusivity between two nodes is stored in a matrix $D_{gb}(i, ii, iii)$, which is consistent with the coordinates. For example, the diffusivity between Node 4 and Node 5 is $D_{gb}(i, ii, 4)$. In the triple junction Node 29, the diffusivity between Node 10 and Node 29 is represented by $D_{gb}(i, ii, 10)$, the diffusivity between Node 28 and Node 29 is represented by $D_{gb}(i, ii, 28)$, and the diffusivity between Node 29 and Node 11 is represented by $D_{gb}(i, ii, 29)$. In the triple junction 1 shown in Figure 3.11, the diffusivity between Node 1 and Node 2 is represented by $D_{gb}(i, ii, 1)$, the diffusivity between Node 19 and Node 1 is represented by $D_{gb}(i, ii, 19)$, and the diffusivity between Node 1 and Node 20 is represented by $D_{gb}(i, ii, 30)$, which is an additional diffusivity.

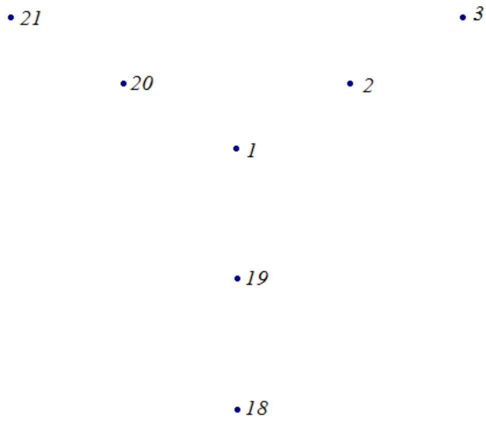

(a) Triple junction at Node 1

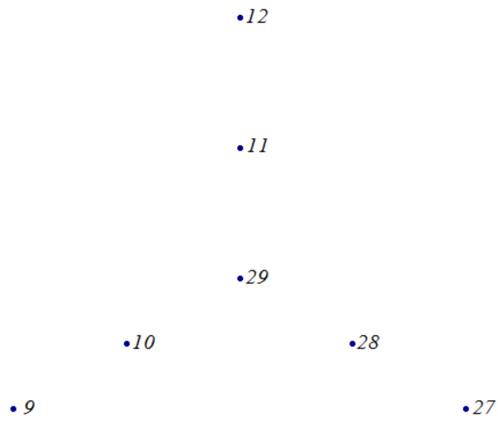

(b) Triple junction at Node 29

Figure 3.11. Triple junctions at Node 1 and Node 29 for equiaxed structure.

3.4 Columnar structure

As discussed in the introduction, the morphology of Sn microstructure is relevant to whiskering propensity. Equiaxed microstructures have lower propensity for whiskering than columnar microstructures, where grains elongate in the film growth direction. To address this, our model also investigated a 2D columnar structure. As seen in Figure 3.12, the standard honeycomb lattice is elongated uniformly in y direction.

3.4.1 Two dimensional network

The two dimensional columnar grain structure network is built based on a grain size of 1 μm wide (in x) and 3 (in y) μm length. The number of Sn grains is decided by Sn film length and thickness. For a Sn film with a length of 35 μm, and a thickness of 6 μm, there are approximately 20 grains along the length direction and 2 grains along the thickness direction, Figure 3.12.

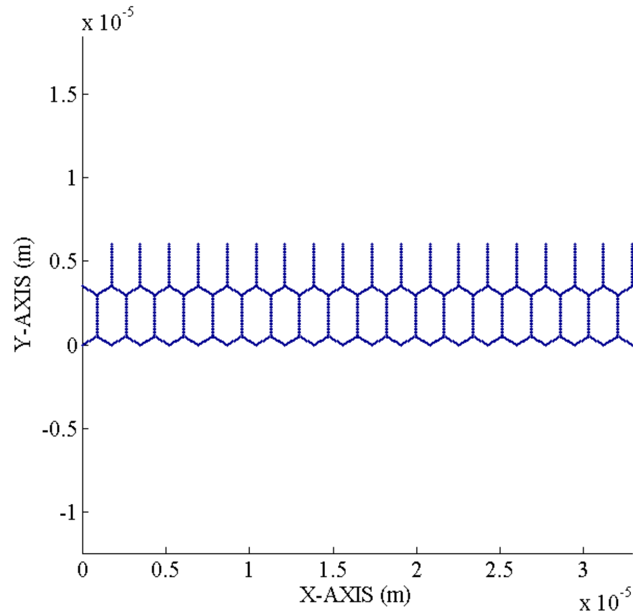

Figure 3.12. Model 2D columnar structure with a length of 35 μm, and a thickness of 6 μm.

3.4.2 Unit cell

Similar to the equiaxed structure, the unit cell is chosen as half of the columnar grain, which is composed of 44 nodes shown in Figure 3.13. The distance between each two neighboring nodes is 0.1 μm. Node 1 and Node 44 are two triple junction nodes connected with other unit cells. Node 1 has three neighboring nodes which are Node 2 in the same cell, Node 34* and Node 35* in the neighboring cell (i.e. the unit cell to the left (-x) and down (-y) from the unit cell shown). Node 44 has three neighboring nodes which are Node 43 in the same cell, Node 10* and Node 11* in the neighboring cell to the left (-x) and up (+y). Similarly, Nodes 34 and 35 are neighbors with Node 1* in the unit cell to the right

(+x) and up (+y); Node 10 to 11 are neighbors with Node 44* in the unit cell to the right (+x) and down (-y).

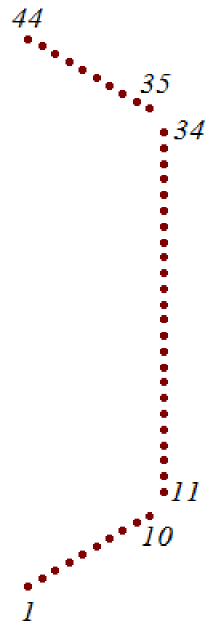

Figure 3.13. Unit cell of columnar structure.

3.4.3 Coordinates

Similar to what was done for the equiaxed structure, a node's position in the columnar network is represented by a Matlab three dimension matrix $x(i, ii, iii)$ and $y(i, ii, iii)$, where i represents the position of the unit cell in x-direction, ii represents the position of the unit cell in y-direction, and iii represents the position of the node inside the unit cell. For the columnar structure model shown in Figure 3.14, the whole network can be distinguished by four different parts. The bottom partial unit cells

are located at $ii = 1$ (green part on the bottom of Figure 3.14). The complete unit cells are located at $ii = 2$ (blue part in Figure 3.14) and the partial unit cells at the top of the structure are located at $ii = 3$ (green part on top of Figure 3.14); also several additional nodes which are required to terminate the structure are located on the top and right boundary (red in Figure 3.14).

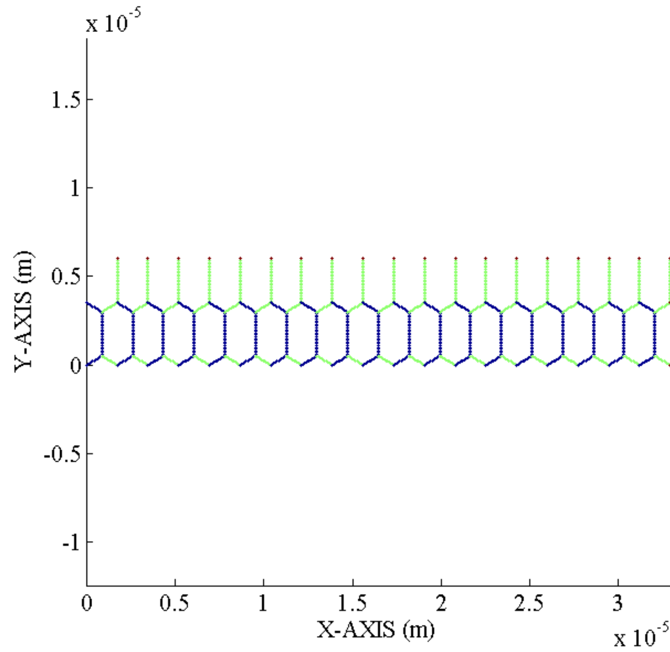

Figure 3.14. Clarification of the nodes comprising the columnar structure in terms of unit cell to which they belong.

Thus, the coordinates of all the nodes can be calculated as,

a. partial unit cells in the bottom $i = 2\ to\ 20, ii = 1, iii = 35\ to\ 44$,

$$x(i, 1, iii) = 1\mu m \times sin60° \times (i - 1) \times 2 - 0.1\mu m \times sin60° \times (iii - 34)$$

$$y(i,1,iii) = 0.1\mu m \times cos60° \times (iii - 34)$$

b. complete cells in the middle of the network $i = 2\ to\ 20,\ ii = 2$,

$$x(i,ii,iii) = 1\mu m \times sin60° \times (i-2) \times 2 + 0.1\mu m \times sin60° \times (iii-1),$$
$$iii = 1\ to\ 10$$

$$x(i,ii,iii) = 1\mu m \times sin60° \times [(i-2) \times 2 + 1], \qquad iii = 11\ to\ 34$$

$$x(i,ii,iii) = 1\mu m \times sin60° \times [(i-2) \times 2 + 1] - 0.1\mu m \times sin60° \times (iii-34),$$
$$iii = 35\ to\ 44$$

$$y(i,ii,iii) = (0.1\mu m \times 25 + 1\mu m \times sin30°) \times (ii-2) + 0.1\mu m \times sin30° \times (iii-1),$$
$$iii = 1\ to\ 10$$

$$y(i,ii,iii) = (0.1\mu m \times 25 + 1\mu m \times sin30°) \times (ii-2) + 1\mu m \times sin30° + 0.1\mu m \times (iii-10), \qquad iii = 11\ to\ 34$$

$$y(i,ii,iii) = (0.1\mu m \times 25 + 1\mu m \times sin30°) \times (ii-1) + 0.1\mu m \times sin30° \times (iii-34), \qquad iii = 35\ to\ 44$$

c. partial unit cell on the top $i = 2\ to\ 20, ii = 3, iii = 1\ to\ 34,$

$$x(i,ii,iii) = 1\mu m \times sin60° \times (i-2) \times 2 + 0.1\mu m \times sin60° \times (iii-1),$$
$$iii = 1\ to\ 10$$

$$x(i, ii, iii) = 1\mu m \times sin60° \times (i-2) \times 2 + 0.1\mu m \times sin60° \times 10, \qquad iii = 11\ to\ 34$$

$$y(i, ii, iii) = (1\mu m + 1\mu m \times sin30°) \times (ii-2) + 0.1\mu m \times sin30° \times (iii-1),$$
$$iii = 1\ to\ 10$$

$$y(i, ii, iii) = (1\mu m + 1\mu m \times sin30°) \times (ii-2) + 1\mu m \times sin30° + 0.1\mu m$$
$$\times (iii-10), \qquad iii = 11\ to\ 34$$

d. additional nodes which complete the network

d-1. nodes on the top $i = 2\ to\ 20,\ \ ii = 4$

$$x(i, 4,1) = 1\mu m \times sin60° \times [(i-2) \times 2 + 1]$$

$$y(i, 4,1) = (0.1\mu m \times 25 + 1\mu m \times sin30°) \times 3$$

d-2. nodes on the right boundary when ii is even,

$$x(21, ii, 1) = 1\mu m \times sin60° \times (20-1) \times 2$$

$$y(21, ii, 1) = (0.1\mu m \times 25 + 1\mu m \times sin30°) \times (ii-2)$$

$$x(21, ii, 44) = 1\mu m \times sin60° \times (20-1) \times 2$$

$$y(21, ii, 44) = (0.1\mu m \times 25 + 1\mu m \times sin30°) \times (ii-1) + 1\mu m \times sin30°$$

3.4.4 Diffusivity

Again, similar to our approach for the equiaxed system, diffusivity between two nodes is represented by $D_{gb}(i, ii, iii)$, which is consistent with the coordinates. For example, the diffusivity between Node 2 and Node 3 is $D_{gb}(i, ii, 2)$. In the triple junction area of Node 44 shown in Figure 3.15, the diffusivity between Node 10 and Node 44 is represented by $D_{gb}(i, ii, 10)$, the diffusivity between Node 43 and Node 44 is represented by $D_{gb}(i, ii, 43)$, and the diffusivity between Node 44 and Node 11 is represented by $D_{gb}(i, ii, 44)$. In the triple junction area of Node 1, the diffusivity between Node 1 and Node 2 is represented by $D_{gb}(i, ii, 1)$, the diffusivity between Node 34 and Node 1 is represented by $D_{gb}(i, ii, 34)$, and the diffusivity between Node 1 and Node 20 is represented by $D_{gb}(i, ii, 45)$, which is an additional diffusivity inserted into the system.

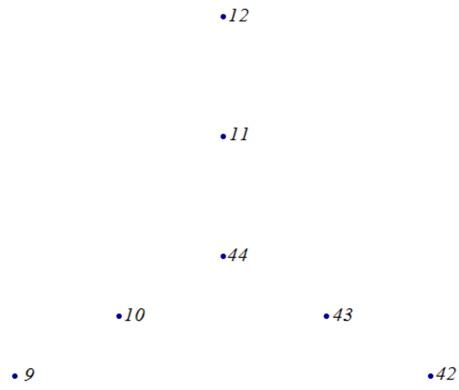

(a) Triple junction at Node 44

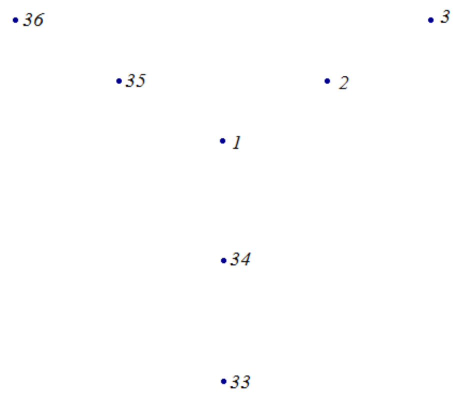

(b) Triple junction at Node 1

Figure 3.15. Triple junctions, Node 1 and Node 44, in columnar structure.

4. Equiaxed grain structure testing

4.1 Equilibrium diffusivity

As a first test of the network models, a fairly simple case is explored; long range elastic stress $\sigma_{L.R.}$ is disregarded, there exists zero externally applied stress throughout the system, an equiaxed structure is modeled, and all nodes forming the bottom (in y) of the network are set to have constant compressive diffusion stress equal to yield stress, which is -15MPa. Such a boundary condition is used as a model to represent intermetallic formation below the film which has caused plastic deformation and forced atoms into the Sn grain boundaries. Thus, grain boundaries near the assumed plastically deformed region (i.e. at the bottom of our model system) are assumed to be in a compressive yield stress state. Furthermore, their stress state is held constant. This mimics a condition where any atoms that diffuse away from these nodes are replaced by additional atoms added to the bottom (boundary condition) nodes. From a physical point of view, the idea is that intermetallic formation continues to provide a supply of new grain boundary atoms due to plastic deformation processes immediately below the Sn thin film. Put simply, the numbers of atoms in this model grain boundary network increases with time. The diffusivities of all the segments are equal, shown in Figure 4.1(b).

As the model is now addressing a 2D representation of a film, these are multiple Sn grains residing at what we consider the film free surface (i.e. the top of the system in y). It is necessary to describe what represents a condition where whisker formation is expected to

occur. At one extreme case of stress evolution, every Sn grain on the surface would be subject to the same stress at all time (i.e. complete uniformity). In such a case, we propose whisker formation would not occur. Conversely, we propose that stress localization near certain Sn surface grains is necessary to drive whiskering. Uniform stress evolution drives uniform deformation whereas localized stress drives localized deformation. Currently, no attempt is made to determine the degree of stress localization required to drive whisker formation and growth. Instead, the model is exercised to determine whether grain boundary diffusion anisotropy can drive stress localization near only certain Sn surface grains.

The total stress in all nodes at certain time steps are shown in Figure 4.2.With the time step 1 second, stress throughout the system increases gradually and fairly uniformly. This behavior is exactly as we expect; uniform diffusivity throughout and a simple static stress boundary condition (without long range stress effect) combine to give very uniform stress evolution with the system approaching zero stress gradient throughout.

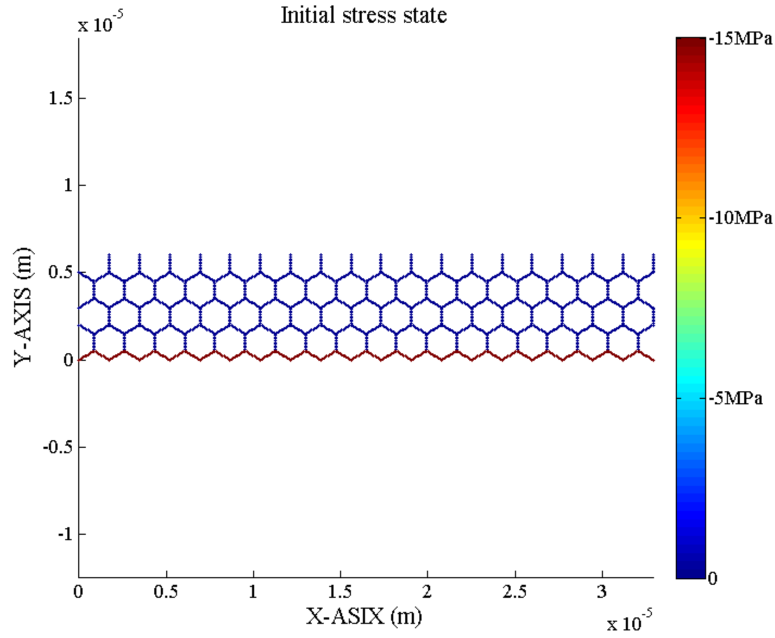

(a) Initial stress state

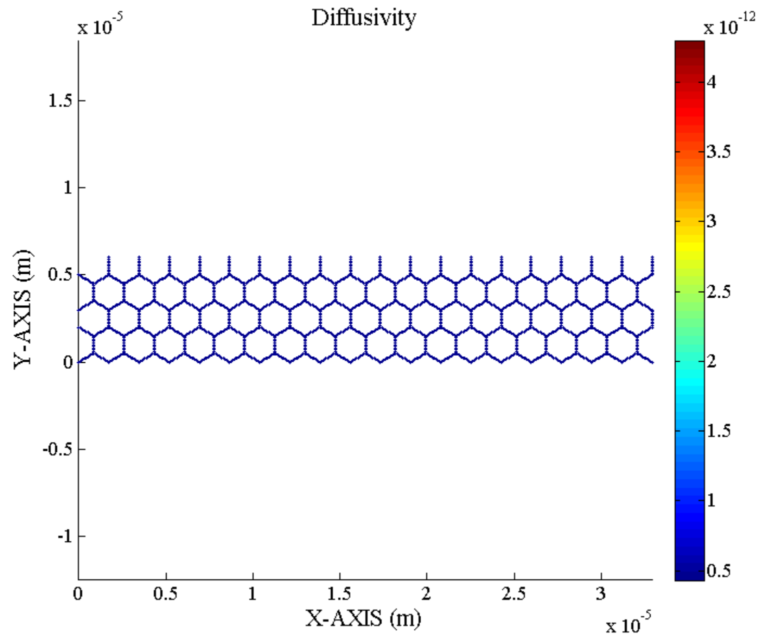

(b) Diffusivity

Figure 4.1. Initial stress state and diffusivity of the uniform diffusivity equiaxed network model. Note that (a) color bar on the right side shows the stress from 0 to -15MPa. (b) Color bar on the right side shows the diffusivity from $4.3 \times 10^{13} m^2/s$ to $4.3 \times 10^{12} m^2/s$ (this model has no variation in δD_{gb}).

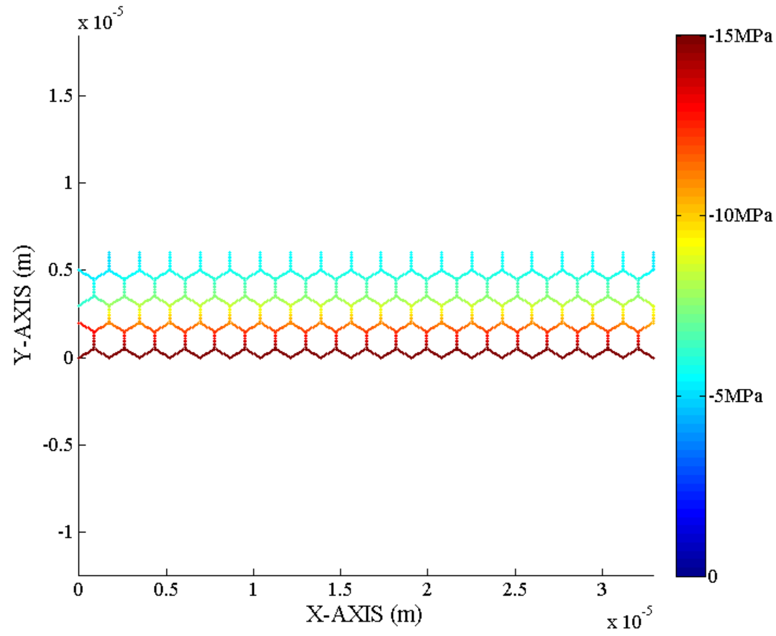

(a) t= 500000

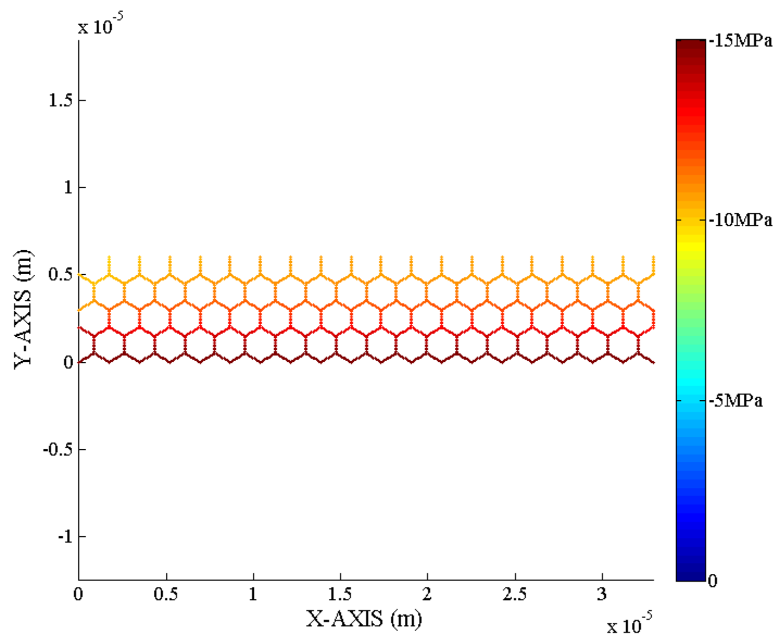

(b) t= 1050000

Figure 4.2. The total stress state of the uniform diffusivity equiaxed model at two different time steps. Note that color bar on the right side shows the stress from 0 to -15MPa.

4.2 Faster diffusivities in central region

Next, we explore a model with anisotropy in the grain boundary diffusivity. This model is very similar to the previous one except the diffusivities of grain boundaries in the central part of the system (i.e. for 1μm < x < 2μm) are set to be $4.3 \times 10^{12} m^2/s$, which is 10 times larger than those in the other part of the network (Figure 4.3). Note this case represents an extreme where fast diffusion grain boundaries are clustered – or localized – in the grain boundary network. In such a case, stress localization should obviously emerge.

As the time step proceeds to t=109429, in the central region of the network, the diffusion is faster, making the stresses more compressive in that region compared to the other part of the network. The surface grains in this region evolve compressive stress much more rapidly compared to other surface grains. Again, it is not surprising that in this simple situation, diffusivity anisotropy can clearly drive stress concentration at certain surface grains. However, the distribution of grain boundary diffusivities in this model is ideal. In a more realistic situation, the possibility that grain boundaries with faster diffusivities cluster as modeled here is likely to be very small. This is because such boundaries are expected to represent a minority faction of grain boundaries present in a given film.

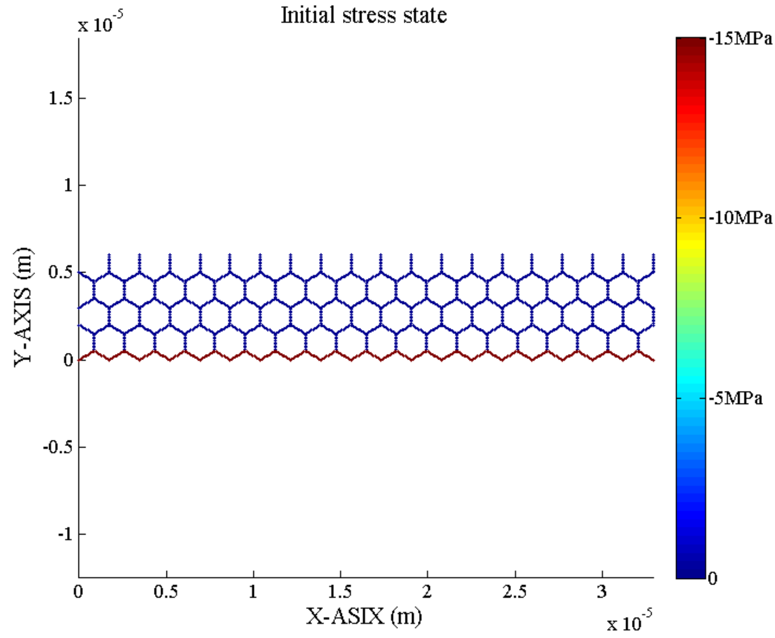

(a) Initial stress state

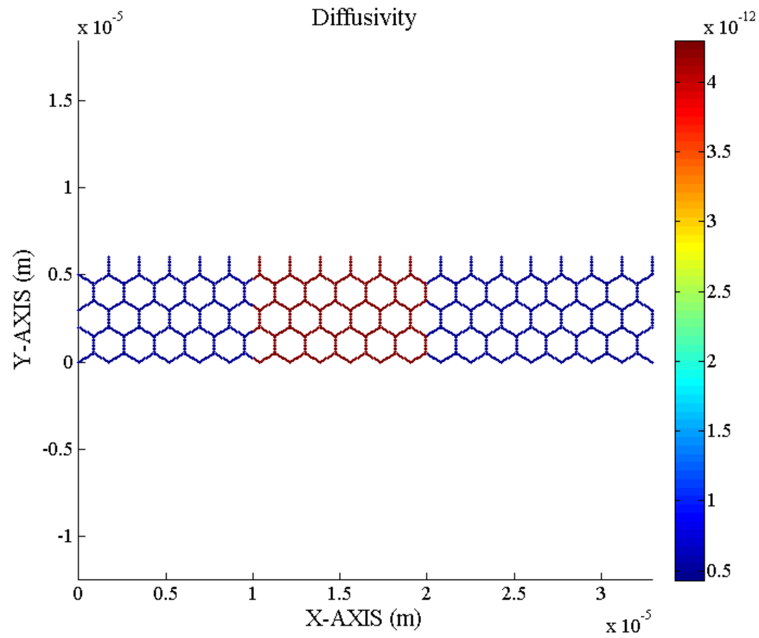

(b) Diffusivity

Figure 4.3. Initial total stress state and diffusivity of the localized faster diffusivities equiaxed model. Note that (a) color bar on the right side shows the stress from 0 to -15MPa. (b) Color bar on the right side shows the diffusivity from $4.3 \times 10^{13} m^2/s$ to $4.3 \times 10^{12} m^2/s$.

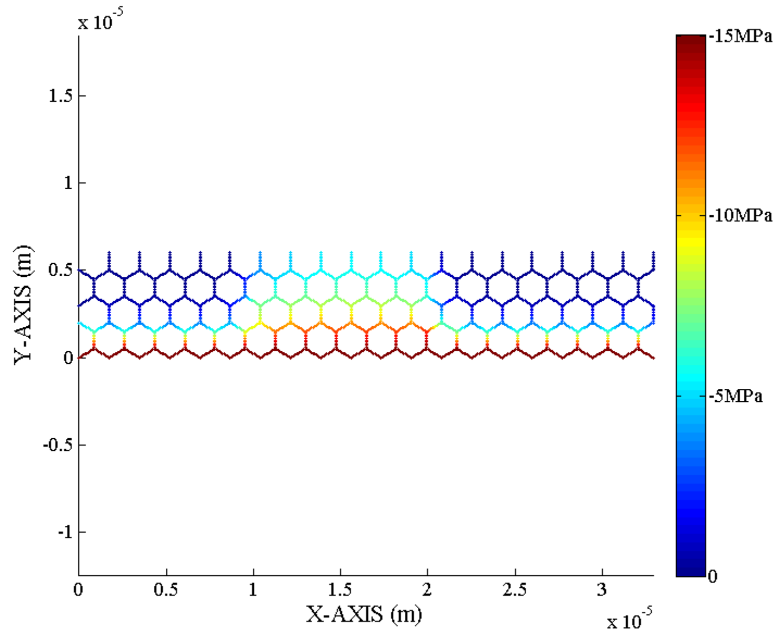

(a) t= 50000

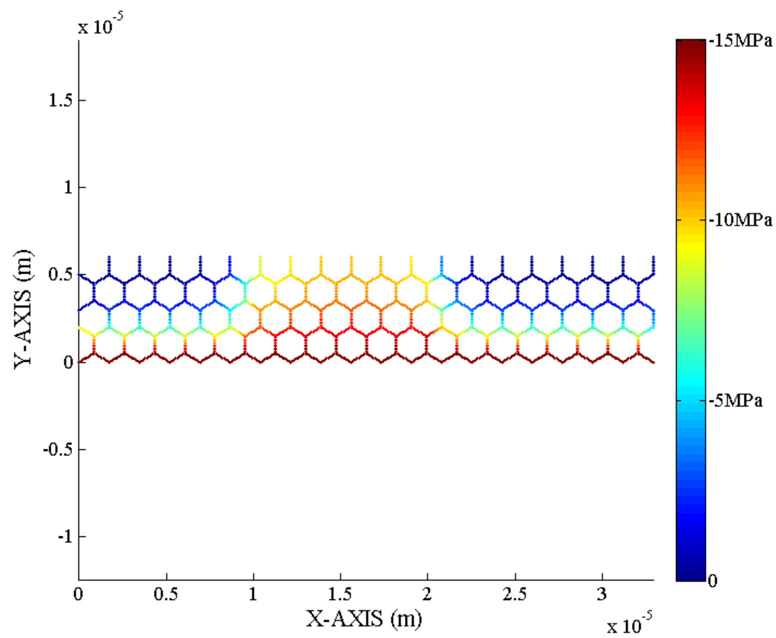

(b) t= 109429

Figure 4.4. The stress state of the localized faster diffusivities equiaxed model at two different times. Note that color bar on the right side shows the stress from 0 to -15MPa.

4.3 10% random segments of faster diffusivities

To introduce greater realism, we assume fast diffusivity grain boundaries are a minority of the network and that they are randomly located. The same boundary conditions as the previous two tests are used. The bottom of the network is set have constant diffusive stress of -15MPa, and other part of the network has zero stress, shown in Figure 4.5. Again, long range elastic contributions are ignored. In the Sn film, the grain boundary diffusivities are randomly populated. In this test, using the Matlab function "randperm" to generate random numbers, 10 percent of the total segments were assigned faster diffusivities.

From Figure 4.6, we can see that the low concentration and randomly distributed faster segments result in a relatively uniform stress increase on the surface grains. In others words, stress evolution throughout the system is more rapid compared with the isotropic diffusivity model but there is no localization of stress at surface grains. Again, we take such localization to be a signature of a whiskering site. As such, we would predict a very low propensity for whiskering in this model case. Note it can be seen that this model can be used to determine how kinetics of stress evolution quantitatively depend upon concentration of fast boundaries. Given that this is a model of grain boundary diffusion where non-trivial connectivity exists, such dependence may not be trivial. For instance, with 10% faster boundaries, is this equivalent to modeling a uniform system with δD_{gb} throughout given by a linear weighted average? If a linear mixing rule applies at low concentration, it would be interesting to determine the concentration where it breaks down,

or if indeed it does. This current study is focused on stress localization so questions such as these – though interesting – are beyond the scope of this thesis. Nonetheless, it can be seen that the presented model is very suitable for carrying out such future research

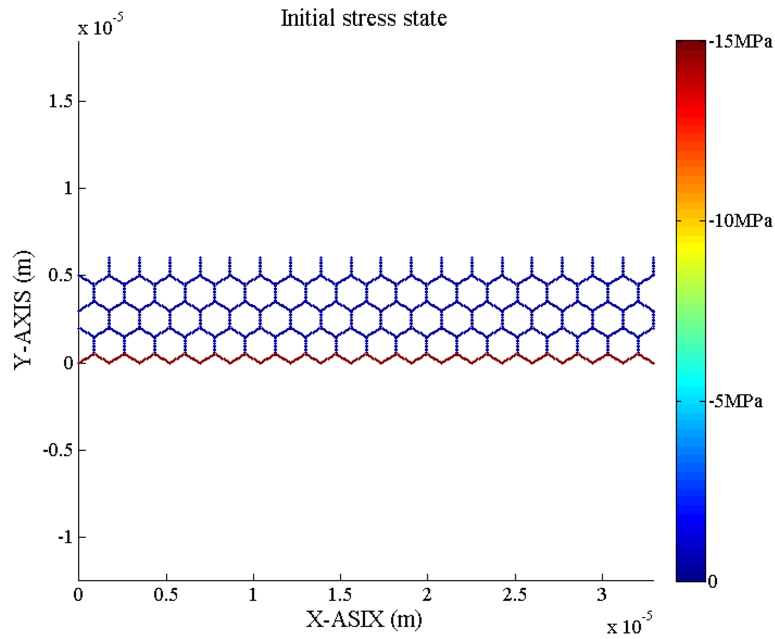

(a) Initial stress state

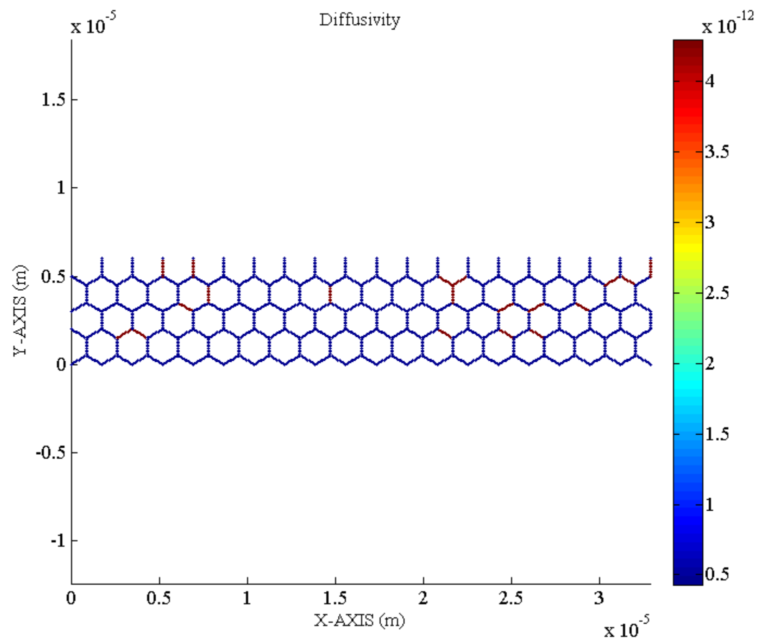

(b) Diffusivity

Figure 4.5. Initial total stress state and diffusivity for the equiaxed 10 percent randomly populated fast grain boundaries system. Note that (a) color bar on the right side shows the stress from 0 to -15MPa. (b) Color bar on the right side shows the diffusivity from $4.3 \times 10^{13} m^2/s$ to $4.3 \times 10^{12} m^2/s$.

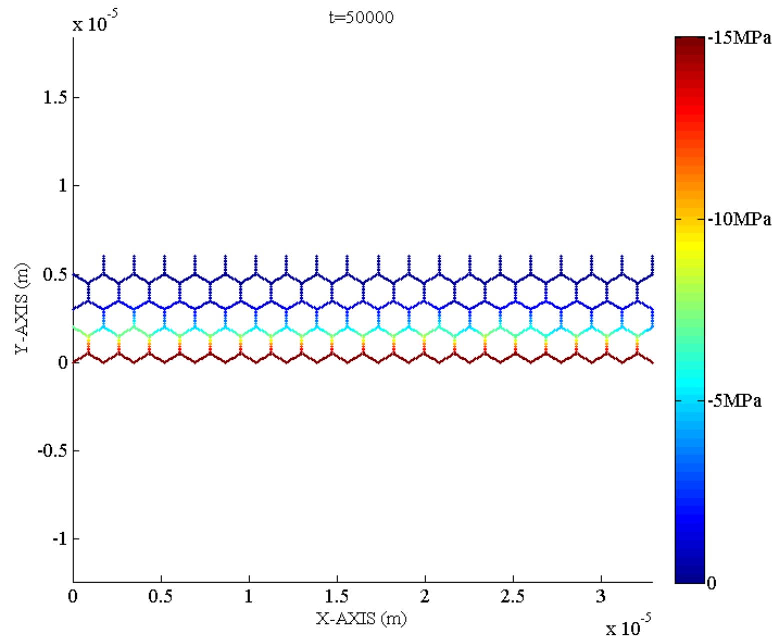

(a) t= 50000

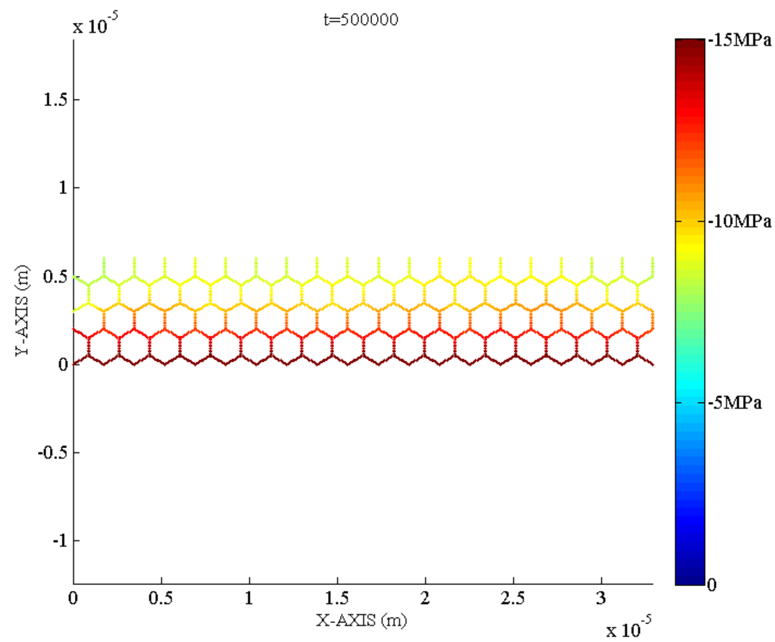

(b) t= 500000

Figure 4.6. The total stress state in the 10 percent randomly populated fast grain boundaries equiaxed model at two different time steps. Note that color bar on the right side shows the stress from 0 to -15MPa.

4.4 33% random segments of faster diffusivities

Similar to the previous case with the 10% grain boundaries having faster diffusivity, in this test 33% of segments are set to have faster diffusivities than others, shown in Figure 4.7. The stress evolution in this test also shows that the faster segments which are fairly uniformly located in the network result in a relatively uniform stress increase on the surface grains. However from Figure 4.8, it is also obvious that a greater degree of stress localization near free surface grains occurs for the higher concentration of fast boundaries.

This is shown quantitatively in Figure 4.9, where total stress for all triple junctions at the base of a surface grain presented. Note, mass transport to any nodes forming the grain boundaries around surface grains must occur through triple junction nodes at the bottom of the surface grains. As such, observing stress in those triple junction nodes gives an indication of the stress state local to each relevant surface grain. A simple interpretation is that, when a triple junction below a given surface grain reaches a stress equal to some critical value, the grain above that triple junction will extrude from the surface. Data are shown for the 10% and 33% fast boundary system; different points in time are shown for each system. Times are chosen when the first surface grain triple junction reaches 70% of yield stress in each system. As can be seen in the figure, greater variation exists in the total stress state near surface grains for the higher concentration fast diffusivity grain boundary system. Also note the time elapsed before a surface triple junction node reaches 70% yield

stress is roughly half for the higher concentration system compared to the 10% fast diffusivity grain boundary system. Greater variation for the 33% system is indicative of greater stress localization near surface grains. This provides evidence that anisotropic grain boundary diffusivity may be a sufficient condition to drive stress localization at a surface grain in a Sn film and thus cause whiskering.

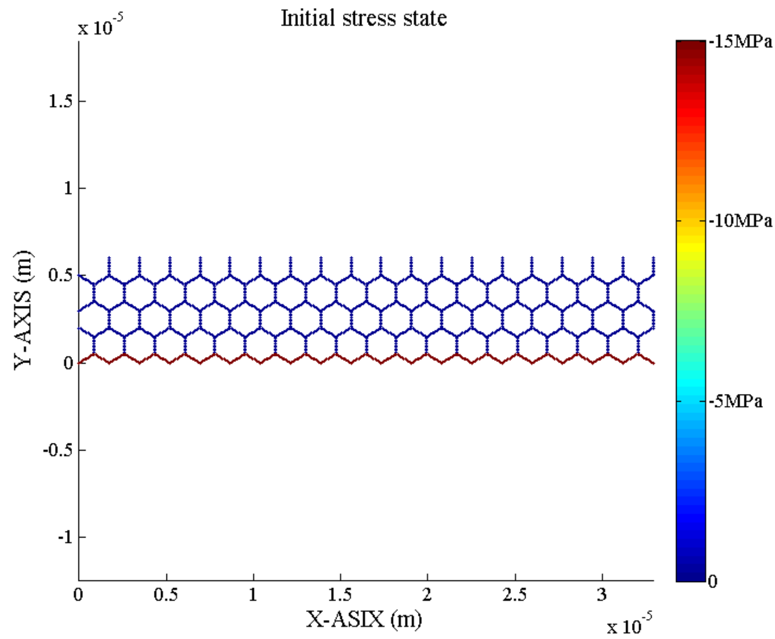

(a) Initial stress state

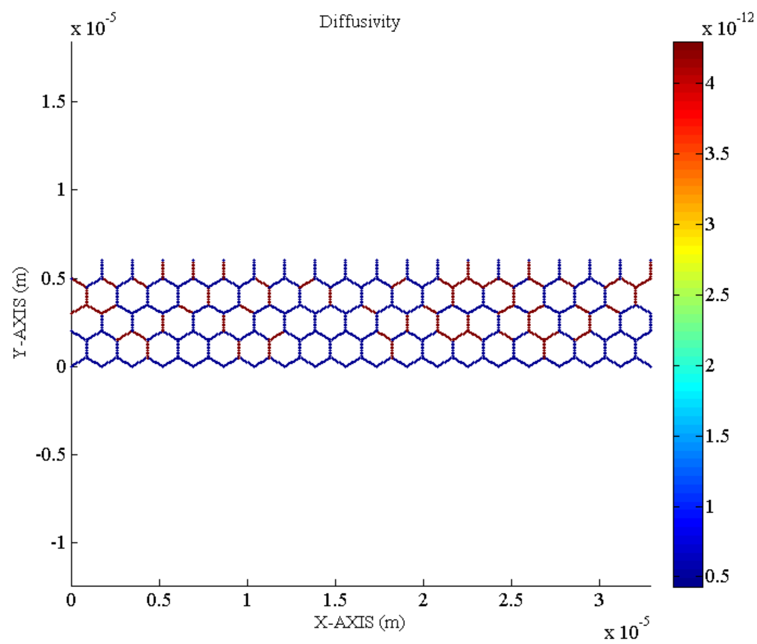

(b) Diffusivity

Figure 4.7. Initial total stress state and diffusivity for the equiaxed, 33 percent randomly populated fast diffusivity grain boundaries. Note that (a) color bar on the right side shows the stress from 0 to -15MPa. (b) Color bar on the right side shows the diffusivity from $4.3 \times 10^{13} m^2/s$ to $4.3 \times 10^{12} m^2/s$.

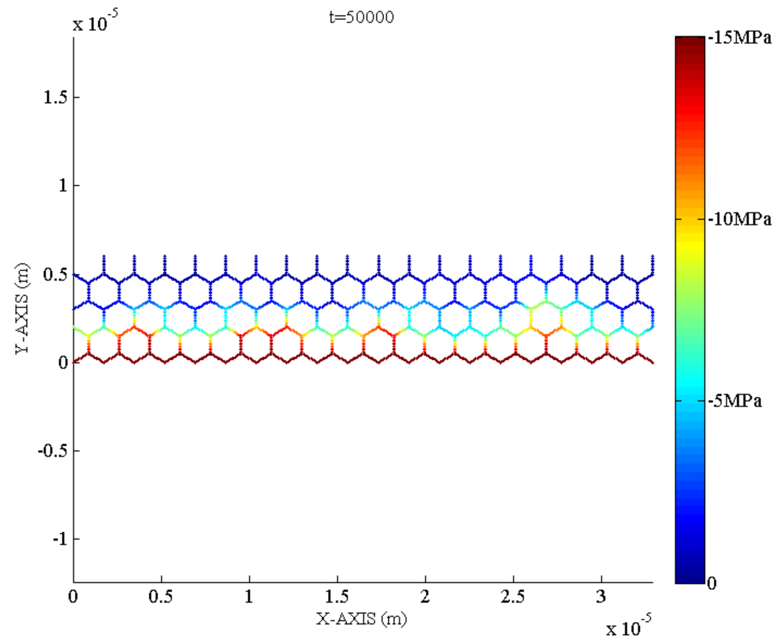

(a) t= 50000

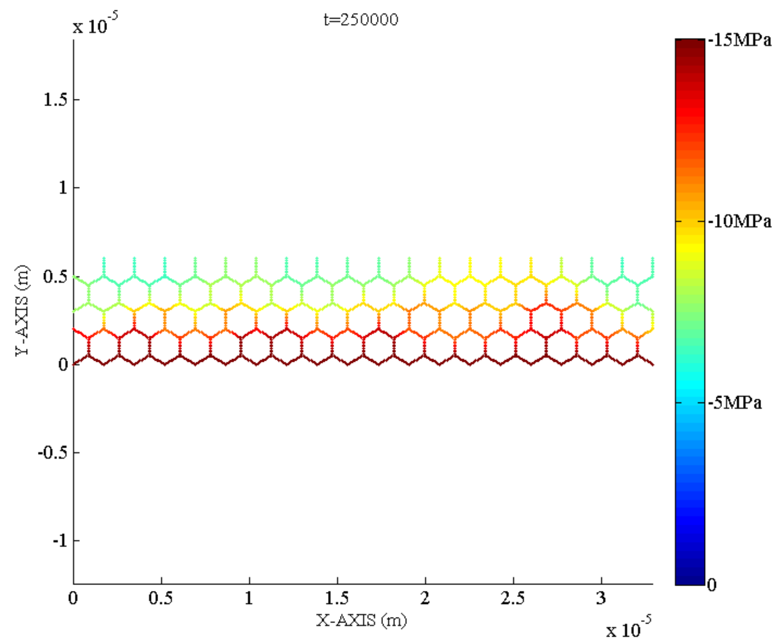

(b) t= 250000

Figure 4.8. The total stress state in the 33 percent randomly populated fast grain boundaries equiaxed model at two different time steps. Note that color bar on the right side shows the stress from 0 to -15MPa.

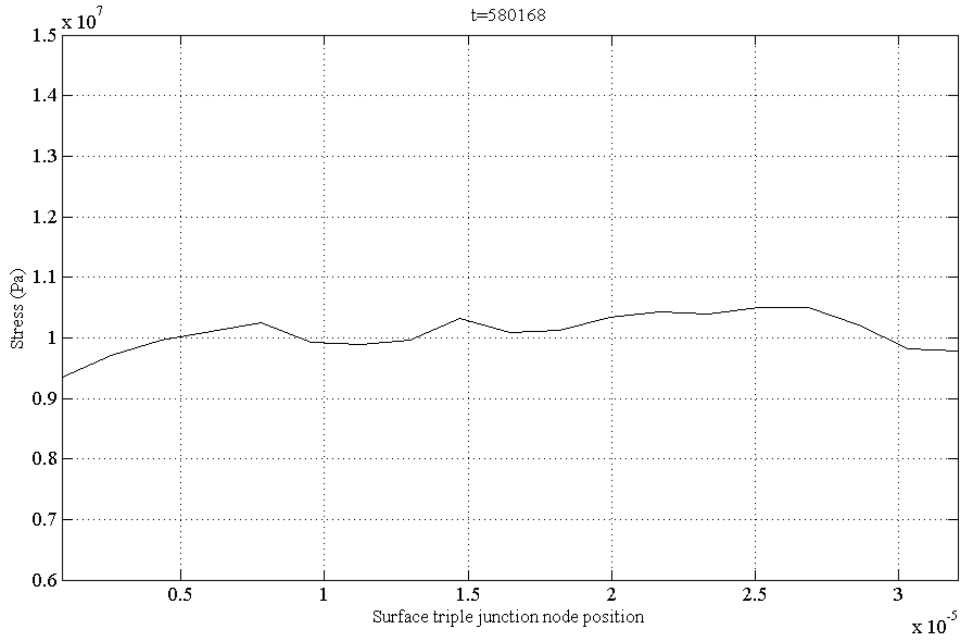

(a) Stress versus surface triple junction node position for system with 10% random segments of faster diffusivities at t=580168s.

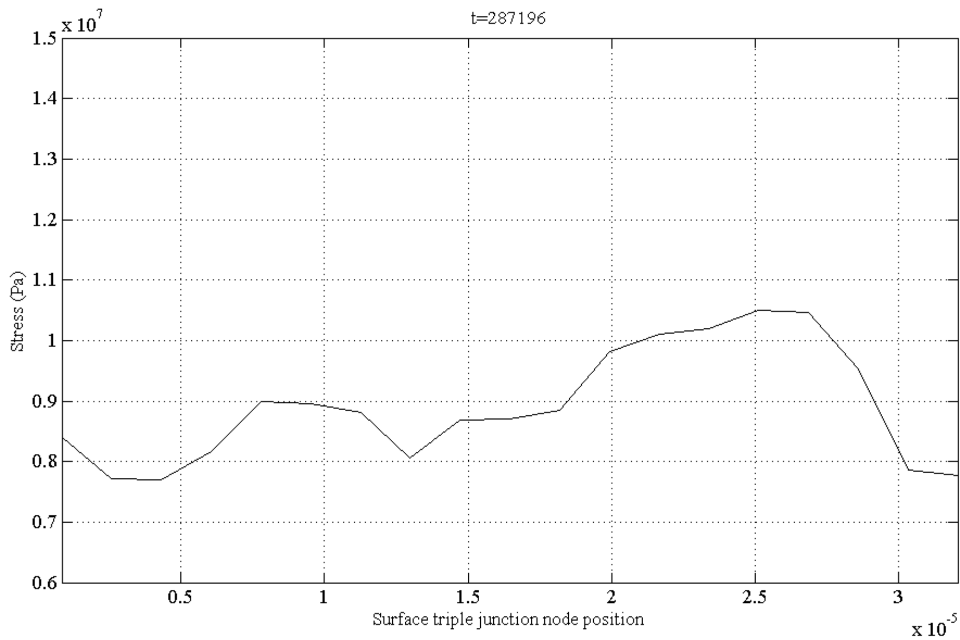

(b) Stress versus surface triple junction node position for system with 33% random segments of faster diffusivities at t=287196s.

Figure 4.9. Total stress state of triple junction nodes at the bottom of the free surface grains, when the first of such nodes reaches 70% of yield.

4.5 Interpretation and perspective

The goal of this thesis was to create and document a numerical model capable of examining the role grain boundary diffusion anisotropy plays in the Sn whisker phenomenon. With this tool now in place and evidence available – albeit, highly preliminary evidence – that grain boundary diffusion anisotropy may play a key role in dictating weather whiskering occurs, more exhausting research must now be done. While such research is beyond the scope of this thesis, some interpretation of existing results is possible. Primarily, we address the question if the time scales for stress evolution in our model are at least reasonable, compared to laboratory observations of Sn whisker growth. For the highest concentration fast diffusion grain boundary system, the first surface triple junction node reached 70% of yield in 287,196s or a little over three days. If we take this as a measure of the order of magnitude of incubation time, then it is quite reasonable, compared to real world observation of Sn whisker growth. Note, observed incubation times span a very broad range (days to years) so this is a relatively easy metric to which our model might be compared. Nonetheless, given that our model is highly simplified (2D, uniform structure, etc.), this is good evidence that our parameters for stress evolution due to atoms entering grain boundaries are reasonable.

5. Conclusion and Future Work

Our main conclusion is we have developed a model capable of examining anisotropic grain boundary diffusion in Sn thin film. We have verified that the model's numerical implementation is robust by examining stress evolution in a number of simple test cases. The 2D model presented captures what we believe to be required ingredients for evaluating if anisotropic grain boundary diffusion alone can drive whiskering. A condition for whiskering assumed here is that stress near surface grains in a film becomes somehow localized such that individual surface grains develop relatively larger magnitude stress, compared to neighboring surface grains. From our tests, a fairly trivial conclusion is that if faster grain boundaries cluster together in a structure, stress localization will occur at surface grains close to a fast boundary cluster. A less trivial conclusion is that randomly distributed fast grain boundaries at sufficient concentration can drive stress localization near certain surface grains. This observation requires further comment.

While it is true that Figure 4.7 shows a degree of stress localization, it is debatable as to the degree of localization required to drive whiskering. For instance, surface triple junctions adjacent to the one with highest magnitude have stress that is not much below the highest value. Thus, perhaps this would not be sufficient stress localization to drive whiskering. Another comment must be made about the random samples examined here. The use of a single sample at each of the concentration studied is highly problematic. To fully understand the behavior of a random distribution, multiple samples must be studied,

each using an independent seed to begin the random selection process. Only in this way can one understand the range of grain boundary ensembles that belong to a given concentration. While more work with this model is clearly warranted, evidence is still encouraging that grain boundary diffusion anisotropy may play a key role in the Sn whisker phenomenon.

Future work will investigate multiple samples for each randomly distributed system. Even the number of samples necessary to properly represent underlying statistics is unknown. Thus, tools will be developed to better elucidate such statistics. With such information in hand, it will be possible to fully reveal the behavior of randomly distributed fast diffusion grain boundaries. For instance – as alluded to in Section 4.3 – we can then understand how underlying diffusivities and concentrations combine to give a mean-field diffusivity. If simple combining rules can be demonstrated to work in certain concentration ranges, it will be of interest to determine in what concentration range they break down. This is essentially a percolation limit study: we propose that, at low and high concentration simple combining rules will work. However, in some intermediary concentration region, percolation behavior will dominate, making simple mixing rules inadequate.

In addition, future work will examine the influence of grain morphology. For instance, columnar structures shown in Section 3 will be studied. Note, this complicates random statistical considerations because two types of boundary lengths exist in that model. It will also be of use to examine effects of film thickness, grain size and long range elastic stress on stress localization and Sn whisker formation.

References

[1] W. E. Minchinton, The British Tinplate Industry: A History. Clarendon Press, Oxford. 1957. Pp1-5.

[2] C.L. Mantell, Ph.D. Tin: Its Mining, Production, Technology, and Applications. Hafner Publishing Company, Inc. 1970. New York, New York. Pp 384-386.

[3] "ITRI. Tin Use Survey 2007", ITRI, Retrieved 2008-11-21.

[4] Gordon L. Robertson (2006). Food packaging. CRC Press. p. 123.

[5] K. G. Compton, A. Mendizza, and S. M. Arnold, "Filamentary growth on metal surfaces –'Whiskers'," Corrosion, vol. 7, pp. 327–334, 1951.

[6] NASA website: http://nepp.nasa.gov/whisker.

[7] Arnold SM, Plating 53, 96 (1966).

[8] Directive 2002/95/EC of the European Parliament and of the Council of 27 January 2003 on the restriction of the use of certain hazardous substances in electrical and electronic equipment. Off. J. Eur. Union L37, 19 (2003).

[9] California Electronic Waste Recycling Act of 2003.

[10] NIST Workshop on Measurement of Stress in Tin and Tin Alloys (without permission)

[11] W. C. Ellis, Trans. Metall. Soc. AIME 236, 872 (1966).

[12] J.W. Osenbach, J.M. DeLucca, B.D. Potterger, A. Amin, R.L. Shook, and F.A. Baiocchi, IEEE Trans. Electron. Packag. Manuf. 30(1), 23 (2007).

[13] Dimitrovska Aleksandra, Kovacevic Radovan, IEEE Trans. Electron. Packag. Manuf, VOL. 33, NO. 3, July 2010 193.

[14] L. Sauter, A. Seekamp, Y. Shibata, Y. Kanameda, H. Yamashita, Microelectronics Reliability 50 (2010) 1631–1635.

[15] NASA website GSFC experiment #4, http://nepp.nasa.gov/whisker/experiment/exp4/index.html.

[16] J. W. Osenbach, Creep and its effect on Sn whisker growth. J. Appl. Phys. 106, 094903 (2009)

[17] P. Harris, International Tin Research ITPI Report No. 724, 1994.

[18] B. D. Dunn, European Space Agency (ESA) Report SRT-223, 1 (1987).

[19] W.J. Boettinger, C.E. Johnson, L.A. Bendersky, K.W. Moon, M.E. Williams, G.R. Stafford, Acta Mater. 53 (2005) 5033.

[20] Onishi M, Fujibuchi H. Trans J Inst Metal 1975;16:539.

[21] Tu KN, Thompson RD. Acta Metall 1982;30:947.

[22] C. C. Wei, P. C. Liu, and Chih Chen, Journal of Applied Physics 102, 043521 (2007)

[23] Sarah M. Miller, Uttara Sahaym, and M. Grant Norton, Metallurgical and Materials Transactions A Volume 41A, December 2010—3387

[24] K.N. Tu, C. Chen, and A.T. Wu: J. Mater. Sci: Mater. Electron.,2007, vol. 18, pp. 269–81.

[25] W. J. Boettinger, C. E. Johnson, L. A. Bendersky, K.-W. Moon, N. E. Williams, and G. R. Stafford, Acta Mater. 53, 5033 _2005_.

[26] K. N. Tu, Mater. Chem. Phys. 46, 217 (1996).

[27] B. Hutchinson, J. Oliver, M. Nylen, and J. Hagstrom, Mater. Sci. Forum 467–470, 465 (2004).

[28] E.J. Buchovecky, N. Jadhav, A.F. Bower, and E. Chason: Finite element modeling of stress evolution in Sn films due to growth of the Cu6Sn5 intermetallic compound. J. Electron. Mater. 38, 2676 (2009).

[29] E.J. Buchovecky, N. Du, and A.F. Bower: A model of Sn whisker growth by coupled plastic flow and grain-boundary diffusion.Appl. Phys. Lett. 94, 191904 (2009).

[30] E. Chason, N. Jadhav, W.L. Chan, L. Reinbold, and K.S. Kumar: Whisker formation in Sn and Pb-Sn coatings: Role of intermetallic growth, stress evolution, and plastic deformation processes. Appl.Phys. Lett. 92, 171901 (2008).

[31] Michael S. Sellers,1 Andrew J. Schultz,1 Cemal Basaran,2 and David A. Kofke: beta-Sn grain-boundary structure and self-diffusivity via molecular dynamics simulations, Physical Review B 81, 134111 (2010)

[32] C. Pao, S. M. Foiles, E. B. Webb III, D. J. Srolovitz, and J. A. Floro, Phys.Rev. Lett. 99, 036102 (2007).

[33] E. Chason, B.W. Sheldon, L.B. Freund, Phys. Rev. Lett. 88 (2002) 156103-1.

[34] F.P. Beer, E.R. Johnston, Jr., J.T. DeWolf, D.F. Mazurek, Mechanics of Materials, Fifth edition. McGraw-Hill, New York. 2009. p.427.

Vita

Yibo Wang was born in Shenyang, China in 1985. He studied at Zhejiang University, China during September 2004 to June 2008. He received the degree of Bachelor of Science in Mechanical Engineering and Automation in Zhejiang University in June 2008. His graduation thesis (project) “Edge-wrapping Machine for The Wire Netting” was awarded Excellent Graduation Thesis (Project) of Zhejiang University in 2008.

From August 2009 to September 2011, he studied in the department of Mechanical Engineering and Mechanics at Lehigh University, US and expects to receive a degree of Master of Science in Computational and Engineering Mechanics.

This thesis was typed by the author.